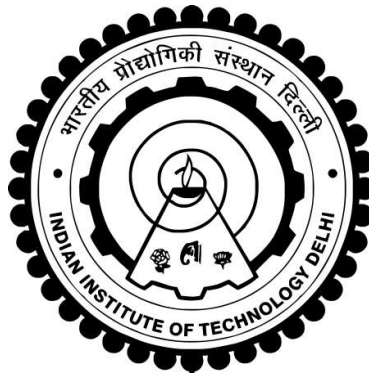


**CONTROL OF AC/DC MICROGRIDS WITH DFIG
BASED WIND ENERGY CONVERSION AND SOLAR
PV GENERATION**

SOUVIK DAS



**DEPARTMENT OF ELECTRICAL ENGINEERING
INDIAN INSTITUTE OF TECHNOLOGY DELHI**

JULY 2023

© Indian Institute of Technology Delhi (IITD), New Delhi, 2023

**CONTROL OF AC/DC MICROGRIDS WITH DFIG BASED
WIND ENERGY CONVERSION AND SOLAR PV
GENERATION**

By

SOUVIK DAS

Department of Electrical Engineering

Submitted

In fulfillment of the requirements of the degree of doctor of philosophy

to the



INDIAN INSTITUTE OF TECHNOLOGY DELHI

JULY 2023

CERTIFICATE

This is to certify that the thesis entitled “**Control of AC/DC Microgrids with DFIG based Wind Energy Conversion and Solar PV Generation,**” being submitted by Mr. **Souvik Das** for the award of the degree of **Doctor of Philosophy** in the Department of Electrical Engineering of Indian Institute of Technology Delhi is a record of a bonafide research work carried out by him under my supervision and guidance. The matter embodied in this thesis has not been submitted for award of any other degree or diploma.

Date: 17-07-2023

(Prof. Bhim Singh)
Department of Electrical Engineering,
Indian Institute of Technology, Delhi

ACKNOWLEDGEMENTS

I wish to express my sincere gratitude and indebtedness to **Prof. Bhim Singh** for providing me valuable guidance and constant supervision to carry out the Ph.D. work. It was a unique and rewarding learning experience to work under him throughout the research period, which has provided me with a deep insight to the world of technical quality research. The commitment, discipline, determination, dedication, resourcefulness and above all innovative approach of Prof. Bhim Singh have been the main inspiration for me to complete this work. His valuable advice, consistent guidance, continuous monitoring and daily encouragement and commitments to achieve excellence have motivated me to improve my work and make best use of my capabilities. It was due to his blessing that I have experienced numerous new traits of technical research that will help me throughout my life.

I express my deep gratitude and sincere thanks to **Prof. Sukumar Mishra, Prof. B. K. Panigrahi and Prof. T. C. Kandpal**, SRC members for their valuable guidance and consistent support throughout my research work. I wish to convey my sincere thanks to **Prof. Bhim Singh, Prof. B. P. Singh, Prof Sukumar Mishra, and Late Prof. Mashuq un Nabi** for their valuable inputs during my course work, which made the strong foundation for my research work. I am grateful to IIT Delhi as an institute for providing me the requisite research facilities.

Thanks are due to Sh. Srichand, Sh. Puran Singh, Mr. Jitendra, Mr. Anurag Kumar, and Mr. Amit Kumar of PG Machine lab and PG Power Electronics lab for providing me facilities and assistance during this work. I am especially thankful to Mr. P. Sambasivaiah, Mr. Jitendra Gupta, Ms. Shalvi Tyagi, Mr. Gaurav Modi, and Mr. Utsav Sharma for their technical support and encouraging suggestions throughout my research work. I am also grateful to all my seniors, Dr. Ikhlaq Hussain, Dr. Shailendra Kumar, Dr. Aniket Anand, Dr. Nidhi Mishra, Dr. Vineet P. Chandran, Dr. Nishant

Kumar, Dr. Sai Pranith Girimaji, Dr. Anjaneesh Mishra, Dr. Piyush Kant, Dr. Saurabh Shukla, Dr. Shadab Murshid, Dr. Deepu Vijay, Dr. Priyank Shah, Dr. V.L. Srinivas, Dr. Sunil Pandey, Dr. Sreejith R, Dr. Shubhra, Dr. Anshul Varshney, Dr. Rohini Sharma, Dr. Pavitra Shukla, Dr. Tipurari Nath Gupta, Dr. Radha Kushwaha, Dr. Shatakshi Sharma, Dr. Seema, Dr. Farheen Chishti, and Dr. Vanadana Jain for being supportive during my stay in IIT Delhi. Moreover, I would like to thank Mr. Gurmeet Singh, Dr. Anjeet Verma, Mr. Debasish Mishra, Dr. Subarni Pradhan, Dr. Tabish Mir, Dr. Utkarsh Sharma, Dr. K. P. Tomar, Ms. Yashi Singh, Ms. Hina Parveen, Ms. Rashmi Rai, Mr. Yalavarthi Amarnath, Mr. Arayadip Sen, Dr. Kashif, Mr. Sudip Bhattacharya, Mr. Bilal Naqvi, Mr. Sandeep Kumar Sahoo, Mr. Vivek Narayanan, Mr. Saran Chaurashiya, Mr. Sayandev Ghosh, Mr. Suri Praneeth, Mr. Priyavrat Vats, Mr. Rahul Kumar, Mr. Sharan Shastri, Mr. Shivam Yadav, Mr. Deepak Saw, Ms. Kousalya V, Ms. Chandrakala Devi, Mr. Saurabh Mishra, Mr. Zarkab Farooqi, Ms. Kripa, Mr. Rohit Kumar, Mr. Vipin Kumar, Mr. Suvom Roy, Mr. Subhadip Chakraborty and all PG Machines lab group for their valuable support.

I would like to thank, Dr. Debargha Brahma and Dr. Arpan Malkhandi and Mr. Jinu Jayachandran who supported and inspired me during my stay in ‘Udaigiri’ house. I would also like to thank Mr. Yatindra Tripathi, Mr. Satish, Mrs. Sunita Verma, Ms. Moni, Mr. Sandeep and all other Electrical Engineering office staff for being supportive throughout my work. I thank all those who have directly or indirectly helped me to complete my dissertation.

The completion of this work was not possible without the blessings of my parents, Mr. Sanjiv Das and Mrs. Emeli Das and my Grandmother Mrs. Arati Das. Their consistent blessings, appreciation and encouragement has emotionally guided the entire journey of my research work. I would like to thank my wife Mrs. Rishul Saxena for giving me the all requisite support and encouragement during my research work. I would like to thank my brother, Mr. Sourabh Das, my sister in law,

Mrs. Monali Paul and other family members for giving me the inner strength and wholehearted support. I would like to thank my brother-in-law, Mr. Palash Saxena and my close friends for their support. The trust in my capabilities, which my family and friends showed in the past few years, has been a key factor to all my achievements. I am indebted to almighty for the blessings to elevate my academic level and granting me the wisdom, health and strength to undertake this research task and enabling me to its completion.

Date: 17-07-2023
Place: New Delhi



Souvik Das

ABSTRACT

The decentralization of electricity generation has initiated a paradigm shift in the power sector. Decentralized generation, in the form of solar photovoltaics (SPVs), wind energy conversion systems (WECSs), etc., when aggregated with local loads, forms a self-sufficient entity, commonly termed a microgrid. Hybrid AC/DC microgrids are rapidly evolving into the preferred microgrid architecture due their minimized power converter redundancy when interfacing the DC-based generation sources or loads. The doubly-fed induction generator (DFIG) shares a large portion of current market share among various variable speed WECSs. This is primarily due to its permanent magnet-free constructional benefits and reduced rating generator-side power converter. When integrated along with the SPV array-based solar energy conversion system (SECS), it provides an effective means of meeting the load power requirement. The DFIG-SPV based AC/DC microgrids may either operate as a grid-integrated entity that enables the import or export of the net power with the utility grid or operate as a standalone system, wherein, the deficit/excess generated power is exchanged with an energy storage system.

This work initially deals with the operation and control of DFIG-SPV based standalone AC/DC microgrid. The preliminary requirement of the standalone system is the effective amplitude and frequency regulations. Moreover, power quality aspects of the standalone voltages and currents amidst the presence of unbalanced and nonlinear AC loads cannot be undermined. This becomes increasingly prominent in case of DFIG-SPV based AC/DC microgrids due to the direct inter-connection of DFIG stator terminals with these abnormal AC loads. Any unregulated operation in such circumstances results in unsymmetrical and harmonics currents in the DFIG. Another major concern in the standalone DFIG-SPV based microgrids pertains to the availability and connection status of the DFIG-based WECS. The disconnection/reconnections instants of the DFIG is required to be smooth, while, the standalone AC as well as DC loads are required to be fed uninterruptedly.

In case of grid-integrated DFIG-SPV based AC/DC microgrids, three major issues are dealt in this thesis. The first issue relates to the uncertainty in the grid, especially in AC/DC microgrids located in rural and remote areas. Although many of the rural areas are declared electrified, the grid continuity in such regions is still a major concern. The need for ensuring a seamless transition between grid-integrated and system islanding operating modes is quite apparent. Furthermore, the

uninterrupted operation of the system during these transitions is also a necessity. The second issue relates to the vulnerability of the grid to sudden power changes in the system. The large ramp-rate power changes in the system may impact the grid voltage amplitude and frequency, especially in the remote and secluded regions, where, the grid-interconnection is through long and weak distribution feeders. Grid-assistive power smoothening approaches need to be supplemented within the microgrid control to minimize the risk of grid instability. The third issue that is addressed, relates to the operation of the DFIG-SPV system amidst the presence of unbalance and distortions in the grid voltages. The non-idealities in the voltages culminate into oscillations in the DFIG torque, DFIG stator power, and injected grid power. Meanwhile, it degrades the power quality of DFIG rotor currents, DFIG stator currents, and injected grid currents. Both control-related and topology-related approaches are required to ensure enhanced operation of the system with the non-ideal grid voltage scenario.

After effectively mitigating the three major issues in the grid-integrated operation of the DFIG-SPV system, this thesis deals with the self-sustainability aspect of the microgrid during prolonged grid outage scenarios. Normally, the energy storage integrated to the microgrid provides sufficient back-up during islanding conditions. However, the energy storage cannot be designed to sustain prolonged periods of grid-outage. Therefore, to maintain the self-sufficiency of the system, the framework for operation of a dispatchable diesel generator system working alongside the WECS and SECS is required. The uninterrupted operation and seamless mode transition are also inculcated in this thesis through the control scheme of diesel generator (DG)-equipped microgrid.

Upon devising the methodology for control and operation of DFIG-SPV-DG based AC/DC microgrid, the focus of the research work shift towards devising generalized methodologies with uninterrupted feature and seamless mode transition for systems with multiple DFIGs and multiple SPV arrays integrated within a well-structured AC/DC microgrid architecture with separate AC and DC subgrids. Initially, control and operation of standalone multiple-source AC/DC microgrids are investigated, which are followed by implementation of grid-integrated multiple-source AC/DC microgrids.

The performance of all the microgrids are examined through simulation and experimental analyses. The obtained results showcase satisfactory control performance for all the features in the AC/DC microgrids comprising of DFIG-based wind energy conversion and solar photovoltaic generation.

सार

बिजली उत्पादन के विकेंद्रीकरण ने बिजली क्षेत्र में एक आदर्श बदलाव की शुरुआत की है। सौर फोटोवोल्टाइक्स (एसपीवी), पवन ऊर्जा रूपांतरण प्रणाली (डब्ल्यूईसीएस) आदि के रूप में विकेंद्रीकृत उत्पादन, जब स्थानीय भार के साथ जोड़ा जाता है, एक आत्मनिर्भर इकाई बनाता है, जिसे आमतौर पर माइक्रोग्रिड कहा जाता है। हाइब्रिड एसी/डीसी माइक्रोग्रिड तेजी से पसंदीदा माइक्रोग्रिड आर्किटेक्चर में विकसित हो रहे हैं क्योंकि डीसी-आधारित पीढ़ी के स्रोतों या भारों को इंटरफेस करते समय उनके न्यूनतम पावर कन्वर्टर अतिरिक्त होते हैं। डबल-फेड इंडक्शन जनरेटर (डीएफआईजी) विभिन्न चर गति डब्ल्यूईसीएस के बीच वर्तमान बाजार हिस्सेदारी का एक बड़ा हिस्सा साझा करता है। यह मुख्य रूप से इसके स्थायी चुंबक-मुक्त निर्माण लाभों और घटी हुई रेटिंग जनरेटर-साइड पावर कन्वर्टर के कारण है। जब एसपीवी सरणी-आधारित सौर ऊर्जा रूपांतरण प्रणाली (एसईसीएस) के साथ एकीकृत किया जाता है, तो यह भार शक्ति की आवश्यकता को पूरा करने का एक प्रभावी साधन प्रदान करता है। डीएफआईजी-एसपीवी आधारित एसी/डीसी माइक्रोग्रिड या तो एक ग्रिड-एकीकृत इकाई के रूप में काम कर सकते हैं जो यूटिलिटी ग्रिड के साथ शुद्ध बिजली के आयात या निर्यात को सक्षम बनाता है या एक स्टैंडअलोन सिस्टम के रूप में काम करता है, जिसमें घाटे/अधिक उत्पन्न बिजली का आदान-प्रदान किया जाता है। एक ऊर्जा भंडारण प्रणाली।

यह काम शुरू में डीएफआईजी-एसपीवी आधारित स्टैंडअलोन एसी/डीसी माइक्रोग्रिड के संचालन और नियंत्रण से संबंधित है। स्टैंडअलोन सिस्टम की प्रारंभिक आवश्यकता प्रभावी आयाम और आवृत्ति नियम है। इसके अलावा, असंतुलित और गैर-रैखिक एसी लोड की उपस्थिति के बीच स्टैंडअलोन वोल्टेज और धाराओं की बिजली गुणवत्ता पहलुओं को कम नहीं किया जा सकता है। डीएफआईजी-एसपीवी आधारित एसी/डीसी माइक्रोग्रिड्स के मामले में डीएफआईजी स्टेटर टर्मिनलों के इन असामान्य एसी लोड के साथ सीधे इंटर-कनेक्शन के कारण यह तेजी से प्रमुख हो जाता है। ऐसी परिस्थितियों में किसी भी अनियमित संचालन का परिणाम डीएफआईजी में असममित और हार्मोनिक धाराओं में होता है। स्टैंडअलोन डीएफआईजी-एसपीवी आधारित माइक्रोग्रिड्स में एक अन्य प्रमुख चिंता डीएफआईजी-आधारित डब्ल्यूईसीएस की उपलब्धता और कनेक्शन स्थिति से संबंधित है। डीएफआईजी के डिस्कनेक्शन/रीकनेक्शन इंस्टेंट सुचारू होने की आवश्यकता है, जबकि स्टैंडअलोन एसी के साथ-साथ डीसी लोड को निर्बाध रूप से फीड करने की आवश्यकता है।

ग्रिड-एकीकृत डीएफआईजी-एसपीवी आधारित एसी/डीसी माइक्रोग्रिड्स के मामले में, इस थीसिस में तीन प्रमुख मुद्दों को निपटाया गया है। पहला मुद्दा ग्रिड में अनिश्चितता से संबंधित है, विशेष रूप से ग्रामीण और दूरस्थ क्षेत्रों में स्थित एसी/डीसी माइक्रोग्रिड में। हालांकि कई ग्रामीण क्षेत्रों को विद्युतीकृत घोषित कर दिया गया है, ऐसे क्षेत्रों में

ग्रिड निरंतरता अभी भी एक प्रमुख चिंता का विषय है। ग्रिड-एकीकृत और सिस्टम आइलैंडिंग ऑपरेटिंग मोड के बीच एक निर्बाध संक्रमण सुनिश्चित करने की आवश्यकता काफी स्पष्ट है। इसके अलावा, इन संक्रमणों के दौरान सिस्टम का निर्बाध संचालन भी एक आवश्यकता है। दूसरा मुद्दा सिस्टम में अचानक बिजली परिवर्तन के लिए ग्रिड की भेद्यता से संबंधित है। सिस्टम में बड़े रैंप-दर बिजली परिवर्तन ग्रिड वोल्टेज आयाम और आवृत्ति को प्रभावित कर सकते हैं, विशेष रूप से दूरस्थ और एकांत क्षेत्रों में, जहां ग्रिड-इंटरकनेक्शन लंबे और कमजोर वितरण फीडरों के माध्यम से होता है। ग्रिड अस्थिरता के जोखिम को कम करने के लिए ग्रिड-सहायक पावर स्मूथनिंग दृष्टिकोणों को माइक्रोग्रिड नियंत्रण के भीतर पूरक करने की आवश्यकता है। तीसरा मुद्दा जिसका समाधान किया गया है, ग्रिड वोल्टेज में असंतुलन और विकृतियों की उपस्थिति के बीच डीएफआईजी-एसपीवी प्रणाली के संचालन से संबंधित है। वोल्टेज में गैर-आदर्शता डीएफआईजी टोक, डीएफआईजी स्टेटर पावर, और इंजेक्शन ग्रिड पावर में दोलनों में समाप्त होती है। इस बीच, यह डीएफआईजी रोटर धाराओं, डीएफआईजी स्टेटर धाराओं, और इंजेक्शन ग्रिड धाराओं की बिजली की गुणवत्ता को कम करता है। गैर-आदर्श ग्रिड वोल्टेज परिदृश्य के साथ सिस्टम के संवर्धित संचालन को सुनिश्चित करने के लिए नियंत्रण-संबंधित और टोपोलॉजी-संबंधित दोनों दृष्टिकोणों की आवश्यकता होती है।

डीएफआईजी-एसपीवी सिस्टम के ग्रिड-एकीकृत संचालन में तीन प्रमुख मुद्दों को प्रभावी ढंग से कम करने के बाद, यह थिसिस लंबे समय तक ग्रिड आउटेज परिदृश्यों के दौरान माइक्रोग्रिड के स्व-स्थिरता पहलू से संबंधित है। आम तौर पर, माइक्रोग्रिड में एकीकृत ऊर्जा भंडारण द्विपीय स्थितियों के दौरान पर्याप्त बैक-अप प्रदान करता है। हालाँकि, ग्रिड-आउटेज की लंबी अवधि को बनाए रखने के लिए ऊर्जा भंडारण को डिज़ाइन नहीं किया जा सकता है। इसलिए, सिस्टम की आत्मनिर्भरता बनाए रखने के लिए, डब्ल्यूईसीएस और एसईसीएस के साथ काम करने वाले डिस्पैचेबल डीजल जनरेटर सिस्टम के संचालन के लिए रूपरेखा की आवश्यकता है। डीजल जनरेटर (डीजी) से लैस माइक्रोग्रिड की नियंत्रण योजना के माध्यम से इस थिसिस में निर्बाध संचालन और निर्बाध मोड संक्रमण भी शामिल है।

डीएफआईजी-एसपीवी-डीजी आधारित एसी/डीसी माइक्रोग्रिड के नियंत्रण और संचालन के लिए कार्यप्रणाली तैयार करने पर, अनुसंधान कार्य का ध्यान अबाधित विशेषता के साथ सामान्यीकृत कार्यप्रणालियों को तैयार करने और कई डीएफआईजी और कई एसपीवी सरणियों के साथ सिस्टम के लिए सीमलेस मोड ट्रांज़िशन के साथ एकीकृत करने की ओर जाता है। अलग-अलग एसी और डीसी सबग्रिड के साथ अच्छी तरह से संरचित एसी/डीसी माइक्रोग्रिड आर्किटेक्चर। प्रारंभ में, स्टैंडअलोन बहु-स्रोत एसी/डीसी माइक्रोग्रिड के नियंत्रण और संचालन की जांच की जाती है, जिसके बाद ग्रिड-एकीकृत बहु-स्रोत एसी/डीसी माइक्रोग्रिड का कार्यान्वयन किया जाता है।

सिमुलेशन और प्रयोगात्मक विश्लेषण के माध्यम से सभी माइक्रोग्रिड्स के प्रदर्शन की जांच की जाती है। प्राप्त परिणाम डीएफआईजी-आधारित पवन ऊर्जा रूपांतरण और सौर फोटोवोल्टिक उत्पादन वाले एसी/डीसी माइक्रोग्रिड्स में सभी सुविधाओं के लिए संतोषजनक नियंत्रण प्रदर्शन दिखाते हैं।

TABLE OF CONTENTS

	Page No.
Certificate	i
Acknowledgements	ii
Abstract	v
Table of Contents	x
List of Figures	xxii
List of Tables	xli
List of Abbreviations	xlii
List of Symbols	xliv
CHAPTER I INTRODUCTION	1–10
1.1 General	1
1.2 State of Art on Wind-Solar AC/DC Microgrid	3
1.2.1 Standalone Wind-Solar AC/DC Microgrid	3
1.2.2 Grid-Integrated Wind-Solar AC/DC Microgrid	4
1.2.3 Wind-Solar AC/DC Microgrid Integrated With Diesel Generator	5
1.2.4 Multi-Source Wind-Solar AC/DC Microgrid	5
1.3 Objectives and Scope of Work	6
1.4 Organization of Thesis	8
CHAPTER II LITERATURE SURVEY	11–29
2.1 General	11
2.2 Review of Solar Energy Conversion Systems	11
2.2.1 MPPT Techniques for SECS	12
2.2.2 Control of SECS With Multifunctional Capability	13
2.3 Review of Wind Energy Conversion Systems	16
2.3.1 MPPT Techniques for WECS	17
2.3.2 DFIG-based WECS and Its Control Operation	18
2.3.2.1 Multifunctional Control Capability	20
2.3.2.2 Encoderless Control Capability	21
2.4 Microgrid with DFIG-Based WECS and SPV Array	21
2.4.1 Challenges Concerning Standalone Microgrid	22
2.4.2 Challenges Concerning Grid-Integrated Microgrid	24
2.5 Identified Research Areas	27
2.6 Conclusions	29

CHAPTER III	CONTROL OF STANDALONE AC/DC MICROGRIDS CONSISTING OF DFIG-BASED WECS AND SPV ARRAY	30–75
3.1	General	30
3.2	Configurations of DFIG-SPV based Standalone AC/DC Microgrids	30
3.2.1	Standalone AC/DC Microgrid with DFIG-based WECS, Double-Stage SECS, and BES	31
3.2.2	Standalone AC/DC Microgrid with DFIG-based WECS, Single-Stage SECS, and BDC Controlled BES	32
3.2.3	Standalone AC/DC Microgrid with DFIG-based WECS, Double-Stage SECS, and BDC Controlled BES	32
3.2.4	Identified Operation Modes and Possible Transition Phases for DFIG-SPV based Standalone AC/DC Microgrids	32
3.3	Design and Selection of Parameters in DFIG-SPV based Standalone AC/DC Microgrids	34
3.3.1	Design and Selection of WECS	34
3.3.1.1	Design of Wind Turbine	34
3.3.1.2	Selection of DFIG Rating	36
3.3.2	Selection of DC-link Voltage and DFIG-side Transformer Rating	36
3.3.3	Selection of SECS	37
3.3.3.1	Selection of SPV Array for Single-Stage SECS	37
3.3.3.2	Selection of SPV Array for Double-Stage SECS	38
3.3.4	Selection of BES Rating	39
3.3.4.1	Selection of BES for Direct Connection With DC-link	39
3.3.4.2	Selection of BES for DC-link Connection Through BDC	39
3.3.5	Design and Selection of Passive Elements in AC/DC Microgrid	40
3.3.5.1	Design of Interfacing Inductors for SSC	40
3.3.5.2	Design of Inductor in BTC	40
3.3.5.3	Design of Inductor in BDC	40
3.3.5.4	Design of Inductor in BKC	41
3.3.5.5	Design of Ripple Filters	41
3.3.5.6	Design of DC-link Capacitor	41
3.3.6	Selection of Device Ratings in VSCs	41
3.3.6.1	Selection of Device Rating in RSC	42
3.3.6.2	Selection of Device Rating in SSC	42
3.4	Selection Criteria for Transition Switch, Operational Strategy and Control Schemes Involved in DFIG-SPV based Standalone AC/DC Microgrids	43

3.4.1	Criteria for Status Selection of S_{SSTS} in DFIG-SPV based Standalone AC/DC Microgrids	43
3.4.2	Operational Strategy for DFIG-SPV based Standalone AC/DC Microgrids	44
3.4.3	Control of DFIG-SPV based Standalone AC/DC Microgrids	45
3.4.3.1	MPPT Technique for WECS	45
3.4.3.2	MPPT Technique for SECS	46
3.4.3.3	Encoderless Stator Flux-based MRAS for DFIG	47
3.4.3.4	Control Scheme for RSC	48
3.4.3.5	Control Scheme for SSC	50
3.4.3.6	Control Scheme for BKC	52
3.4.3.7	Control Scheme for BTC	52
3.4.3.8	Control Scheme for BDC	53
3.5	MATLAB Modelling for Simulation of DFIG-SPV based Standalone AC/DC Microgrids	53
3.6	Experimental Implementation of DFIG-SPV based Standalone AC/DC Microgrids	53
3.7	Results and Discussion	55
3.7.1	Performance of Standalone AC/DC Microgrid with DFIG-based WECS, Double-Stage SECS, and BES	55
3.7.1.1	Simulation Performance	56
3.7.1.2	Experimental Performance	57
3.7.2	Performance of Standalone AC/DC Microgrid with DFIG-based WECS, Single-Stage SECS, and BDC Controlled BES	62
3.7.2.1	Simulation Performance	62
3.7.2.2	Experimental Performance	64
3.7.3	Performance of Standalone AC/DC Microgrid with DFIG-based WECS, Double-Stage SECS, and BDC Controlled BES	68
3.7.3.1	Simulation Performance	69
3.7.3.2	Experimental Performance	69
3.7.4	Performance of Encoderless Stator Flux-based MRAS for DFIG	74
3.8	Conclusions	75

CHAPTER IV CONTROL OF AC/DC MICROGRIDS CONSISTING OF DFIG-BASED WECS AND SPV ARRAY WITH GRID INTEGRATED AT DFIG STATOR TERMINALS

76–144

4.1	General	76
4.2	Configurations of DFIG-SPV based AC/DC Microgrids With Grid Integrated at DFIG Stator Terminals	77
4.2.1	AC/DC Microgrid Consisting of DFIG-based WECS, Double-Stage SECS, and BES With Grid Integrated at DFIG Stator	77
4.2.2	AC/DC Microgrid Consisting of DFIG-based WECS, Single-Stage SECS, and BDC Controlled BES With Grid Integrated at DFIG Stator	77
4.2.3	AC/DC Microgrid Consisting of DFIG-based WECS, Double-Stage SECS, and BDC Controlled BES With Grid Integrated at DFIG Stator	79
4.2.4	Identified Operation Modes and Possible Transition Phases for DFIG-SPV based AC/DC microgrid With Grid Integrated at DFIG Stator	79
4.3	Selection of Parameters in DFIG-SPV based AC/DC Microgrids With Grid Integrated at DFIG Stator Terminals	80
4.4	Selection Criteria for Transition Switches, Operational Strategy and Control Schemes Involved in DFIG-SPV based AC/DC Microgrids With Grid Integrated at DFIG Stator Terminals	82
4.4.1	Criteria for Status Selection of G_{SSTS} and S_{SSTS} in DFIG-SPV based AC/DC Microgrids With Grid Integrated at DFIG Stator Terminals	82
4.4.2	Operational Strategy for DFIG-SPV based AC/DC Microgrids With Grid Integrated at DFIG Stator Terminals	85
4.4.3	Control of DFIG-SPV based AC/DC Microgrids With Grid Integrated at DFIG Stator Terminals	86
4.4.3.1	Control Scheme for RSC	86
4.4.3.2	Control Scheme for SSC	89
4.5	Enhanced Operation of DFIG-SPV based AC/DC Microgrids With DFIG Stator Interconnected to Non-Ideal Grid	91
4.5.1	Multi-Target Control for Enhanced Operation at Non-Ideal Grid	92
4.5.1.1	System Modelling for Multi-Target Control	92
4.5.1.2	Control Schemes for Enhanced Operation	95
4.5.2	Flexible Control for Enhanced Operation at Non-Ideal Grid	99
4.5.2.1	Control Schemes for Enhanced Operation	100
4.5.3	Adaptive Control for Enhanced Operation at Non-Ideal Grid	103
4.5.3.1	System Modelling for Adaptive Control	104
4.5.3.2	Control Schemes for Enhanced Operation	106

4.6	MATLAB Modelling for Simulation of DFIG-SPV based AC/DC Microgrids With Grid Integrated at DFIG Stator Terminals	108
4.7	Experimental Implementation of DFIG-SPV based AC/DC Microgrids With Grid Integrated at DFIG Stator Terminals	108
4.8	Results and Discussion	110
4.8.1	Performance of AC/DC Microgrid Consisting of DFIG-based WECS, Double-Stage SECS, and BES With Grid Integrated at DFIG Stator	110
4.8.1.1	Simulation Performance	110
4.8.1.2	Experimental Performance	110
4.8.2	Performance of AC/DC Microgrid Consisting of DFIG-based WECS, Single-Stage SECS, and BDC Controlled BES with Grid Integrated at DFIG Stator	117
4.8.2.1	Simulation Performance	117
4.8.2.2	Experimental Performance	120
4.8.3	Performance of AC/DC Microgrid Consisting of DFIG-based WECS, Double-Stage SECS, and BDC Controlled BES with Grid Integrated at DFIG Stator	125
4.8.3.1	Simulation Performance	126
4.8.3.2	Experimental Performance	127
4.8.4	Performance of Multi-Target Control for Enhanced Operation at Non-Ideal Grid	133
4.8.5	Performance of Flexible Control for Enhanced Operation at Non-Ideal Grid	137
4.8.6	Performance of Adaptive Control for Enhanced Operation at Non-Ideal Grid	141
4.9	Conclusions	144

CHAPTER V CONTROL OF AC/DC MICROGRIDS CONSISTING OF DFIG-BASED WECS AND SPV ARRAY WITH GRID INTEGRATED AT ALTERNATE PCI TERMINALS 145–197

5.1	General	145
5.2	Configurations of DFIG-SPV based AC/DC Microgrids With Grid Integrated at Alternate PCI Terminals	146
5.2.1	AC/DC Microgrid Consisting of DFIG-based WECS, Double-Stage SECS, and BES With Grid Integrated at Alternate PCI	146

5.2.2	AC/DC Microgrid Consisting of DFIG-based WECS, Single-Stage SECS, and BDC Controlled BES With Grid Integrated at Alternate PCI	147
5.2.3	AC/DC Microgrid Consisting of DFIG-based WECS, Double-Stage SECS, and BDC Controlled BES With Grid Integrated at Alternate PCI	147
5.2.4	Identified Operation Modes and Possible Transition Phases for DFIG-SPV based AC/DC microgrid With Grid Integrated at Alternate PCI	148
5.3	Design and Selection of Parameters in DFIG-SPV based AC/DC Microgrids With Grid Integrated at Alternate PCI Terminals	151
5.3.1	Design of Interfacing Inductors for GSC	151
5.3.2	Selection of Grid-side Transformer Rating	151
5.3.3	Selection of Device Rating in GSC	151
5.4	Selection Criteria for Transition Switches, Operational Strategy and Control Schemes Involved in DFIG-SPV based AC/DC Microgrids With Grid Integrated at Alternate PCI Terminals	153
5.4.1	Criteria for Status Selection of S_{SSTS} and G_{SSTS} in AC/DC Microgrids With Grid Integrated at Alternate PCI Terminals	153
5.4.2	Operational Strategy for DFIG-SPV based AC/DC Microgrids With Grid Integrated at Alternate PCI Terminals	155
5.4.3	Control of DFIG-SPV based AC/DC Microgrids With Grid Integrated at Alternate PCI Terminals	156
5.4.3.1	Control Scheme for RSC	156
5.4.3.2	Control Scheme for SSC	157
5.4.3.3	Control Scheme for GSC	159
5.5	Approaches for Grid Power Smoothing Amidst Varying Conditions in DFIG-SPV based AC/DC Microgrids	161
5.5.1	Constant Current Injection based GSC Control for Grid Power Smoothing	162
5.5.2	Exponential Estimate based GSC Control for Grid Power Smoothing	163
5.5.3	Ramp-Rate Limit based GSC Control for Grid Power Smoothing	165
5.6	MATLAB Modelling for Simulation of DFIG-SPV based AC/DC Microgrids With Grid Integrated at Alternate PCI Terminals	166
5.7	Experimental Implementation of DFIG-SPV based AC/DC Microgrids with Grid Integrated at Alternate PCI Terminals	167

5.8	Results and Discussion	167
5.8.1	Performance of AC/DC Microgrid Consisting of DFIG-based WECS, Double Stage SECS, and BES With Grid Integrated at Alternate PCI	167
5.8.1.1	Simulation Performance	168
5.8.1.2	Experimental Performance	169
5.8.2	Performance of AC/DC Microgrid Consisting of DFIG-based WECS, Single Stage SECS, and BDC Controlled BES With Grid Integrated at Alternate PCI	175
5.8.2.1	Simulation Performance	175
5.8.2.2	Experimental Performance	177
5.8.3	Performance of AC/DC Microgrid Consisting of DFIG-based WECS, Double Stage SECS, and BDC Controlled BES With Grid Integrated at Alternate PCI	183
5.8.3.1	Simulation Performance	183
5.8.3.2	Experimental Performance	184
5.8.4	Performance of Constant Current Injection based GSC Control for Grid Power Smoothing	190
5.8.5	Performance of Exponential Estimate based GSC Control for Grid Power Smoothing	191
5.8.6	Performance of Ramp-Rate Limit based GSC Control for Grid Power Smoothing	193
5.9	Conclusions	196

CHAPTER VI CONTROL OF AC/DC MICROGRIDS CONSISTING OF DFIG-BASED WECS, SPV ARRAY AND DG-SET WITH GRID INTEGRATED AT ALTERNATE PCI TERMINALS AND DG-SET INTEGRATED AT DFIG STATOR TERMINALS 198–246

6.1	General	198
6.2	Configurations of DFIG-SPV-DG based AC/DC Microgrids With Grid Integrated at Alternate PCI Terminals and DG-Set Integrated at DFIG Stator Terminals	199
6.2.1	AC/DC Microgrid Consisting of DFIG-based WECS, Double-Stage SECS, DG-set, and BES With Grid Integrated at Alternate PCI and DG-Set Integrated at DFIG Stator	199

6.2.2	AC/DC Microgrid Consisting of DFIG-based WECS, Single-Stage SECS, DG-set, and BDC Controlled BES With Grid Integrated at Alternate PCI and DG-Set Integrated at DFIG Stator	201
6.2.3	AC/DC Microgrid Consisting of DFIG-based WECS, Double-Stage SECS, DG-set, and BDC Controlled BES With Grid Integrated at Alternate PCI and DG-Set Integrated at DFIG Stator	202
6.2.4	Identified Operation Modes and Possible Transition Phases for DFIG-SPV-DG based AC/DC microgrid With Grid Integrated at Alternate PCI and DG-Set Integrated at DFIG Stator	202
6.3	Selection of Parameters in DFIG-SPV-DG based AC/DC Microgrids With Grid Integrated at Alternate PCI Terminals and DG-Set Integrated at DFIG Stator Terminals	205
6.4	Selection Criteria for Transition Switches, Operational Strategy and Control Schemes Involved in DFIG-SPV-DG based AC/DC Microgrids With Grid Integrated at Alternate PCI Terminals and DG-Set Integrated at DFIG Stator Terminals	206
6.4.1	Criteria for Status Selection of S _{SSTS} , G _{SSTS} and D _{SSTS} in DFIG-SPV-DG based AC/DC Microgrids With Grid Integrated at Alternate PCI and DG-Set Integrated at DFIG Stator	206
6.4.2	Operational Strategy for DFIG-SPV-DG based AC/DC Microgrids With Grid Integrated at Alternate PCI and DG-Set Integrated at DFIG Stator	208
6.4.3	Control of DFIG-SPV-DG based AC/DC Microgrids With Grid Integrated at Alternate PCI and DG-Set Integrated at DFIG Stator	210
6.4.3.1	Control Scheme for GSC	210
6.4.3.2	Control Scheme for RSC	212
6.4.3.3	Control Scheme for SSC	213
6.5	Incentivized Control of DFIG-SPV-DG based AC/DC Microgrids Through TOUEP Mechanism	215
6.6	MATLAB Modelling for Simulation of DFIG-SPV-DG based AC/DC Microgrids With Grid Integrated at Alternate PCI Terminals and DG-Set Integrated at DFIG Stator Terminals	216
6.7	Experimental Implementation of DFIG-SPV-DG based AC/DC Microgrids With Grid Integrated at Alternate PCI Terminals and DG-Set Integrated at DFIG Stator Terminals	216
6.8	Results and Discussion	217

6.8.1	Performance of AC/DC Microgrid Consisting of DFIG-based WECS, Double Stage SECS, DG-set, and BES with Grid Integrated at Alternate PCI and DG-Set Integrated at DFIG Stator	218
6.8.1.1	Simulation Performance	218
6.8.1.2	Experimental Performance	219
6.8.2	Performance of AC/DC Microgrid Consisting of DFIG-based WECS, Single Stage SECS, DG-set, and BDC Controlled BES With Grid Integrated at Alternate PCI and DG-Set Integrated at DFIG Stator	227
6.8.2.1	Simulation Performance	227
6.8.2.2	Experimental Performance	227
6.8.3	Performance of AC/DC Microgrid Consisting of DFIG-based WECS, Double Stage SECS, DG-set, and BDC Controlled BES With Grid Integrated at Alternate PCI and DG-Set Integrated at DFIG Stator	236
6.8.3.1	Simulation Performance	237
6.8.3.2	Experimental Performance	237
6.8.4	Performance of Incentivized Control in Grid-Integrated State Through ToUEP Mechanism	244
6.9	Conclusions	246
 CHAPTER VII CONTROL OF STANDALONE AC/DC MICROGRIDS CONSISTING OF MULTIPLE DFIG-BASED WECSs AND MULTIPLE SPV ARRAYS		247–272
7.1	General	247
7.2	Configurations of Multiple-Source DFIG-SPV based Standalone AC/DC Microgrids	247
7.2.1	Multiple-Source DFIG-SPV based Standalone AC/DC Microgrid With Additional Battery-Side Converter	248
7.2.2	Multiple-Source DFIG-SPV based Standalone AC/DC Microgrid Without Additional Battery-Side Converter	249
7.3	Selection of Parameters in Multiple-Source DFIG-SPV based Standalone AC/DC Microgrids	249
7.4	Control Schemes Involved in Multiple-Source DFIG-SPV based Standalone AC/DC Microgrid With Additional Battery-Side Converter	250
7.4.1	Control Scheme for BSC	250
7.4.2	Control Scheme for ILC	251

7.4.3	Control Scheme for RSC of q^{th} -DFIG	252
7.4.4	Control Scheme for SSC of q^{th} -DFIG	253
7.5	Control Schemes Involved in Multiple-Source DFIG-SPV based Standalone AC/DC Microgrid Without Additional Battery-Side Converter	254
7.5.1	Control Scheme for ILC	254
7.6	MATLAB Modelling for Simulation of Multiple-Source DFIG-SPV based Standalone AC/DC Microgrids	255
7.7	Experimental Implementation of Multiple-Source DFIG-SPV based Standalone AC/DC Microgrids	255
7.8	Results and Discussion	256
7.8.1	Performance of Multiple-Source DFIG-SPV based Standalone AC/DC Microgrid With Additional Battery-Side Converter	258
7.8.1.1	Simulation Performance	258
7.8.1.2	Experimental Performance	260
7.8.2	Performance of Multiple-Source DFIG-SPV based Standalone AC/DC Microgrid Without Additional Battery-Side Converter	263
7.8.2.1	Simulation Performance	264
7.8.2.2	Experimental Performance	267
7.9	Conclusions	271
 CHAPTER VIII CONTROL OF GRID-INTEGRATED AC/DC MICROGRIDS CONSISTING OF MULTIPLE DFIG-BASED WECSs AND MULTIPLE SPV ARRAYS		273–313
8.1	General	273
8.2	Configurations of Multiple-Source DFIG-SPV based Grid-Integrated AC/DC Microgrids	274
8.2.1	Multiple-Source DFIG-SPV based AC/DC Microgrids With Grid Integrated at DFIGs' Stator Terminals	274
8.2.2	Multiple-Source DFIG-SPV based AC/DC Microgrids With Grid Integrated at Alternate Interconnection Terminals	275
8.2.3	Multiple-Source DFIG-SPV-DG based AC/DC Microgrids With Grid Integrated at Alternate Interconnection Terminals and DG-Set Integrated at DFIGs' Stator Terminals	275
8.3	Selection of Parameters in Multiple-Source DFIG-SPV based Grid-Integrated AC/DC Microgrids	276
8.4	Control Schemes Involved in Multiple-Source DFIG-SPV based AC/DC Microgrids With Grid Integrated at DFIGs' Stator Terminals	276

8.4.1	Control Scheme for ILC	277
8.5	Control Schemes Involved in Multiple-Source DFIG-SPV based AC/DC Microgrids With Grid Integrated at Alternate Interconnection Terminals	279
8.5.1	Control Scheme for ILC	279
8.5.4	Control Scheme for GSC	280
8.6	Control Schemes Involved in Multiple-Source DFIG-SPV-DG based AC/DC Microgrids With Grid Integrated at Alternate Interconnection Terminals and DG-Set Integrated at DFIGs' Stator Terminals	281
8.6.1	Control Scheme for ILC	282
8.7	MATLAB Modelling for Simulation of Multiple-Source DFIG-SPV based Grid-Integrated AC/DC Microgrids	283
8.8	Experimental Implementation of Multiple-Source DFIG-SPV based Grid-Integrated AC/DC Microgrids	283
8.9	Results and Discussion	284
8.9.1	Performance of Multiple-Source DFIG-SPV based AC/DC Microgrids With Grid Integrated at DFIGs' Stator Terminals	284
8.9.1.1	Simulation Performance	285
8.9.1.2	Experimental Performance	289
8.9.2	Performance of Multiple-Source DFIG-SPV based AC/DC Microgrids With Grid Integrated at Alternate Interconnection Terminals	294
8.9.2.1	Simulation Performance	294
8.9.2.2	Experimental Performance	298
8.9.3	Performance of Multiple-Source DFIG-SPV-DG based AC/DC Microgrids With Grid Integrated at Alternate Interconnection Terminals and DG-Set Integrated at DFIGs' Stator Terminals	302
8.9.3.1	Simulation Performance	303
8.9.3.2	Experimental Performance	306
8.10	Conclusions	312
CHAPTER IX MAIN CONCLUSIONS AND SUGGESTIONS FOR FURTHER WORK		314–321
9.1	General	314
9.2	Main Conclusions	315
9.3	Suggestions for Further Work	320
REFERENCES		322–342

APPENDICES	343–346
LIST OF PUBLICATIONS	347–350
BIO-DATA	351

LIST OF FIGURES

- Fig. 3.1 Configuration of standalone AC/DC microgrid with DFIG-based WECS, double-stage SECS, and BES
- Fig. 3.2 Configuration of standalone AC/DC microgrid with DFIG-based WECS, single-stage SECS, and BDC controlled BES
- Fig. 3.3 Configuration of standalone AC/DC microgrid with DFIG-based WECS, double-stage SECS, and BDC controlled BES
- Fig. 3.4 Identified operation modes of DFIG-SPV based standalone AC/DC microgrids
- Fig. 3.5 Selection criteria for computing status of S_{SSTS} DFIG-SPV based standalone AC/DC microgrids
- Fig. 3.6 Operational strategy for DFIG-SPV based standalone AC/DC microgrids
- Fig. 3.7 Incremental conductance MPPT technique for SECS
- Fig. 3.8 Stator flux-based MRAS technique for encoderless operation of DFIG
- Fig. 3.9 Control scheme for RSC in DFIG-SPV based standalone AC/DC microgrids
- Fig. 3.10 Control scheme for SSC in DFIG-SPV based standalone AC/DC microgrids
- Fig. 3.11 Control scheme for BKC in DFIG-SPV based standalone AC/DC microgrids
- Fig. 3.12 Control scheme for BTC in DFIG-SPV based standalone AC/DC microgrids
- Fig. 3.13 Control scheme for BDC in DFIG-SPV based standalone AC/DC microgrids
- Fig. 3.14 Screenshot for simulation of DFIG-SPV based standalone AC/DC microgrids in MATLAB
- Fig. 3.15 Snapshot of experimental prototype of DFIG-SPV based standalone AC/DC microgrids
- Fig. 3.16 Simulation performance of standalone AC/DC microgrid with DFIG-based WECS, double-stage SECS, and BES
- Fig. 3.17 MPPT performance of SPV array in standalone AC/DC microgrid with DFIG-based WECS, double-stage SECS, and BES
- Fig. 3.18 MPPT performance of wind turbine in standalone AC/DC microgrid with DFIG-based WECS, double-stage SECS, and BES
- Fig. 3.19 Dynamic performance at varying wind speed and solar irradiation in standalone AC/DC microgrid with DFIG-based WECS, double-stage SECS, and BES
- Fig. 3.20 Test results displaying commencement of DFIG reconnection in standalone AC/DC microgrid with DFIG-based WECS, double-stage SECS, and BES at TP-I
- Fig. 3.21 Test results displaying DFIG reconnection in standalone AC/DC microgrid with DFIG-based WECS, double-stage SECS, and BES at TP-I
- Fig. 3.22 Test results displaying seamless transition in standalone AC/DC microgrid with DFIG-based WECS, double-stage SECS, and BES at TP-II
- Fig. 3.23 Power quality performance of standalone AC/DC microgrid with DFIG-based WECS, double-stage SECS, and BES with abnormal AC load

- Fig. 3.24 Dynamic performance of standalone AC/DC microgrid with DFIG-based WECS, double-stage SECS, and BES during load changes
- Fig. 3.25 Simulation performance of standalone AC/DC microgrid with DFIG-based WECS, single-stage SECS, and BDC controlled BES during TP-I
- Fig. 3.26 Simulation performance of standalone AC/DC microgrid with DFIG-based WECS, single-stage SECS, and BDC controlled BES during TP-II
- Fig. 3.27 MPPT performance of SPV array in standalone AC/DC microgrid with DFIG-based WECS, single-stage SECS, and BDC controlled BES
- Fig. 3.28 Steady-state waveforms and parameters of DFIG-based WECS in standalone AC/DC microgrid with DFIG-based WECS, single-stage SECS, and BDC controlled BES
- Fig. 3.29 Dynamic performance at varying wind speed and solar irradiation in standalone AC/DC microgrid with DFIG-based WECS, single-stage SECS, and BDC controlled BES
- Fig. 3.30 Test results displaying commencement of DFIG reconnection in standalone AC/DC microgrid with DFIG-based WECS, single-stage SECS, and BDC controlled BES at TP-I
- Fig. 3.31 Test results displaying DFIG reconnection in standalone AC/DC microgrid with DFIG-based WECS, single-stage SECS, and BDC controlled BES at TP-I
- Fig. 3.32 Test results displaying seamless transition in standalone AC/DC microgrid with DFIG-based WECS, single-stage SECS, and BDC controlled BES at TP-II
- Fig. 3.33 Power quality performance of standalone AC/DC microgrid with DFIG-based WECS, single-stage SECS, and BDC controlled BES with abnormal AC load
- Fig. 3.34 Dynamic performance of standalone AC/DC microgrid with DFIG-based WECS, single-stage SECS, and BDC controlled BES during load changes
- Fig. 3.35 Simulation performance of standalone AC/DC microgrid with DFIG-based WECS, double-stage SECS, and BDC controlled BES
- Fig. 3.36 MPPT performance of SPV array in standalone AC/DC microgrid with DFIG-based WECS, double-stage SECS, and BDC controlled BES
- Fig. 3.37 Dynamic performance at varying wind speed and solar irradiation in standalone AC/DC microgrid with DFIG-based WECS, double-stage SECS, and BDC controlled BES
- Fig. 3.38 Test results displaying commencement of DFIG reconnection in standalone AC/DC microgrid with DFIG-based WECS, double-stage SECS, and BDC controlled BES at TP-I
- Fig. 3.39 Test results displaying DFIG reconnection in standalone AC/DC microgrid with DFIG-based WECS, double-stage SECS, and BDC controlled BES at TP-I
- Fig. 3.40 Test results displaying seamless transition in standalone AC/DC microgrid with DFIG-based WECS, double-stage SECS, and BDC controlled BES at TP-II

- Fig. 3.41 Power quality performance of standalone AC/DC microgrid with DFIG-based WECS, double-stage SECS, and BDC controlled BES with abnormal AC load
- Fig. 3.42 Dynamic performance of standalone AC/DC microgrid with DFIG-based WECS, double-stage SECS, and BDC controlled BES during load changes
- Fig. 3.43 Effectiveness of DFIG encoderless operation based on stator flux MRAS at varying wind condition
- Fig. 4.1 Configuration of AC/DC microgrid consisting of DFIG-based WECS, double-stage SECS, and BES with grid integrated at DFIG stator
- Fig. 4.2 Configuration of AC/DC microgrid consisting of DFIG-based WECS, single-stage SECS, and BDC controlled BES with grid integrated at DFIG stator
- Fig. 4.3 Configuration of AC/DC microgrid consisting of DFIG-based WECS, double-stage SECS, and BDC controlled BES with grid integrated at DFIG stator
- Fig. 4.4 Identified operation modes of DFIG-SPV based AC/DC microgrids with grid integrated at DFIG stator
- Fig. 4.5 Selection criteria for computing status of G_{SSTS} in DFIG-SPV based AC/DC microgrids with grid integrated at DFIG stator
- Fig. 4.6 Selection criteria for computing status of S_{SSTS} in DFIG-SPV based AC/DC microgrids with grid integrated at DFIG stator
- Fig. 4.7 Operational strategy for DFIG-SPV based AC/DC microgrids with grid integrated at DFIG stator
- Fig. 4.8 Control scheme for RSC in DFIG-SPV based AC/DC microgrids with grid integrated at DFIG stator
- Fig. 4.9 Control scheme for SSC in DFIG-SPV based AC/DC microgrids with grid integrated at DFIG stator
- Fig. 4.10 Non-ideal grid voltages processing through MRHGI-HE
- Fig. 4.11 Control scheme of RSC for enhanced operation at non-ideal grid through multi-target approach
- Fig. 4.12 Control scheme of SSC for enhanced operation at non-ideal grid through multi-target approach
- Fig. 4.13 Non-ideal grid voltages processing through C_{ext} SOGI-HSS
- Fig. 4.14 Control scheme of RSC for enhanced operation at non-ideal grid through flexible control approach
- Fig. 4.15 Control scheme of SSC for enhanced operation at non-ideal grid through flexible control approach
- Fig. 4.16 Control scheme of RSC for enhanced operation at non-ideal grid through adaptive control approach
- Fig. 4.17 Control scheme of SSC for enhanced operation at non-ideal grid through adaptive control approach
- Fig. 4.18 Screenshot for simulation of DFIG-SPV based AC/DC microgrids with grid integrated at DFIG stator in MATLAB

- Fig. 4.19 Snapshot of experimental prototype of DFIG-SPV based AC/DC microgrids with grid integrated at DFIG stator
- Fig. 4.20 Simulation performance of AC/DC microgrid consisting of DFIG-based WECS, double-stage SECS, and BES with grid integrated at DFIG stator
- Fig. 4.21 MPPT performance of SPV array in AC/DC microgrid consisting of DFIG-based WECS, double-stage SECS, and BES with grid integrated at DFIG stator
- Fig. 4.22 Steady-state waveforms and indices of DFIG at a wind speed of 6.44m/s in AC/DC microgrid consisting of DFIG-based WECS, double-stage SECS, and BES with grid integrated at DFIG stator
- Fig. 4.23 Dynamic performance at varying wind speed and solar irradiation in AC/DC microgrid consisting of DFIG-based WECS, double-stage SECS, and BES with grid integrated at DFIG stator
- Fig. 4.24 Test results displaying uninterrupted operation and seamless transition in AC/DC microgrid consisting of DFIG-based WECS, double-stage SECS, and BES with grid integrated at DFIG stator at TP-I and TP-III
- Fig. 4.25 Test results displaying uninterrupted operation and seamless transition in AC/DC microgrid consisting of DFIG-based WECS, double-stage SECS, and BES with grid integrated at DFIG stator at TP-II
- Fig. 4.26 Test results displaying uninterrupted operation and seamless transition in AC/DC microgrid consisting of DFIG-based WECS, double-stage SECS, and BES with grid integrated at DFIG stator at TP-IV
- Fig. 4.27 Test results displaying uninterrupted operation and seamless transition in AC/DC microgrid consisting of DFIG-based WECS, double-stage SECS, and BES with grid integrated at DFIG stator at TP-V and TP-VI
- Fig. 4.28 Test results displaying uninterrupted operation and seamless transition in AC/DC microgrid consisting of DFIG-based WECS, double-stage SECS, and BES with grid integrated at DFIG stator at TP-VII and TP-VIII
- Fig. 4.29 Power quality performance at abnormal AC load of AC/DC microgrid consisting of DFIG-based WECS, double-stage SECS, and BES with grid integrated at DFIG stator
- Fig. 4.30 Dynamic performance of AC/DC microgrid consisting of DFIG-based WECS, double-stage SECS, and BES with grid integrated at DFIG stator during load changes
- Fig. 4.31 Simulation performance of AC/DC microgrid consisting of DFIG-based WECS, single-stage SECS, and BDC controlled BES with grid integrated at DFIG stator during TP-VI, TP-I, TP-IV, and TP-VII
- Fig. 4.32 Simulation performance of AC/DC microgrid consisting of DFIG-based WECS, single-stage SECS, and BDC controlled BES with grid integrated at DFIG stator during TP-V, TP-VIII, TP-III, and TP-II
- Fig. 4.33 MPPT performance of SPV array in AC/DC microgrid consisting of DFIG-based WECS, single-stage SECS, and BDC controlled BES with grid integrated at DFIG stator

- Fig. 4.34 Steady-state waveforms and parameters of DFIG-based WECS in AC/DC microgrid consisting of DFIG-based WECS, single-stage SECS, and BDC controlled BES with grid integrated at DFIG stator
- Fig. 4.35 Dynamic performance at varying wind speed and solar irradiation in AC/DC microgrid consisting of DFIG-based WECS, single-stage SECS, and BDC controlled BES with grid integrated at DFIG stator
- Fig. 4.36 Test results displaying uninterrupted operation and seamless transition in AC/DC microgrid consisting of DFIG-based WECS, single-stage SECS, and BDC controlled BES with grid integrated at DFIG stator at TP-I and TP-III
- Fig. 4.37 Test results displaying uninterrupted operation and seamless transition in AC/DC microgrid consisting of DFIG-based WECS, single-stage SECS, and BDC controlled BES with grid integrated at DFIG stator at TP-II
- Fig. 4.38 Test results displaying uninterrupted operation and seamless transition in AC/DC microgrid consisting of DFIG-based WECS, single-stage SECS, and BDC controlled BES with grid integrated at DFIG stator at TP-IV
- Fig. 4.39 Test results displaying uninterrupted operation and seamless transition in AC/DC microgrid consisting of DFIG-based WECS, single-stage SECS, and BDC controlled BES with grid integrated at DFIG stator at TP-V and TP-VI
- Fig. 4.40 Test results displaying uninterrupted operation and seamless transition in AC/DC microgrid consisting of DFIG-based WECS, single-stage SECS, and BDC controlled BES with grid integrated at DFIG stator at TP-VII and TP-VIII
- Fig. 4.41 Power quality performance of AC/DC microgrid consisting of DFIG-based WECS, single-stage SECS, and BDC controlled BES with grid integrated at DFIG stator amidst abnormal AC load
- Fig. 4.42 Dynamic performance of AC/DC microgrid consisting of DFIG-based WECS, single-stage SECS, and BDC controlled BES with grid integrated at DFIG stator during load changes
- Fig. 4.43 Simulation performance of AC/DC microgrid consisting of DFIG-based WECS, double-stage SECS, and BDC controlled BES with grid integrated at DFIG stator
- Fig. 4.44 MPPT performance of SPV array in AC/DC microgrid consisting of DFIG-based WECS, double-stage SECS, and BDC controlled BES with grid integrated at DFIG stator
- Fig. 4.45 Dynamic performance at varying wind speed and solar irradiation in AC/DC microgrid consisting of DFIG-based WECS, double-stage SECS, and BDC controlled BES with grid integrated at DFIG stator
- Fig. 4.46 Test results displaying uninterrupted operation and seamless transition in AC/DC microgrid consisting of DFIG-based WECS, double-stage SECS, and BDC controlled BES with grid integrated at DFIG stator at TP-I and TP-III
- Fig. 4.47 Test results displaying uninterrupted operation and seamless transition in AC/DC microgrid consisting of DFIG-based WECS, double-stage SECS, and BDC controlled BES with grid integrated at DFIG stator at TP-II

- Fig. 4.48 Test results displaying uninterrupted operation and seamless transition in AC/DC microgrid consisting of DFIG-based WECS, double-stage SECS, and BDC controlled BES with grid integrated at DFIG stator at TP-IV
- Fig. 4.49 Test results displaying uninterrupted operation and seamless transition in AC/DC microgrid consisting of DFIG-based WECS, double-stage SECS, and BDC controlled BES with grid integrated at DFIG stator at TP-V and TP-VI
- Fig. 4.50 Test results displaying uninterrupted operation and seamless transition in AC/DC microgrid consisting of DFIG-based WECS, double-stage SECS, and BDC controlled BES with grid integrated at DFIG stator at TP-VII and TP-VIII
- Fig. 4.51 Test results to assess stator and grid currents injection behaviour as regulated by RSC and SSC operation
- Fig. 4.52 Power quality performance of AC/DC microgrid consisting of DFIG-based WECS, double-stage SECS, and BDC controlled BES with grid integrated at DFIG stator amidst abnormal AC load
- Fig. 4.53 Dynamic performance of AC/DC microgrid consisting of DFIG-based WECS, double-stage SECS, and BDC controlled BES with grid integrated at DFIG stator during load changes
- Fig. 4.54 Test results displaying performance improvements with DT-I and DT-II targets at unbalanced voltages
- Fig. 4.55 Test results displaying performance improvements with DT-I and DT-II targets at distorted voltages
- Fig. 4.56 Test results displaying performance improvement with DT-III and DT-IV targets at unbalanced voltages
- Fig. 4.57 Test results displaying performance improvement with DT-III and DT-IV targets at distorted voltages
- Fig. 4.58 Test results displaying performance improvement with GT-I, GT-II and GT-III targets at unbalanced voltages
- Fig. 4.59 Test results displaying performance improvement with GT-I and GT-III targets at distorted voltages
- Fig. 4.60 Test results displaying performance improvement with GT-II target at distorted voltages
- Fig. 4.61 Performance of flexible second-order torque ripple minimization technique at unbalanced grid voltages
- Fig. 4.62 Performance of flexible sixth-order torque ripple minimization technique at distorted grid voltages
- Fig. 4.63 Performance of flexible second-order grid active power ripple minimization technique at unbalanced grid voltages
- Fig. 4.64 Performance of flexible sixth-order grid active power ripple minimization technique at distorted grid voltages
- Fig. 4.65 Non-ideal grid voltages used for control performance evaluation

- Fig. 4.66 Performance analysis of DFIG torque ripple mitigation strategy at non-ideal grid voltages
- Fig. 4.67 Performance analysis of grid power ripple mitigation strategy at non-ideal grid voltages
- Fig. 5.1 Configuration of AC/DC microgrid consisting of DFIG-based WECS, double-stage SECS, and BES with grid integrated at alternate PCI
- Fig. 5.2 Configuration of AC/DC microgrid consisting of DFIG-based WECS, single-stage SECS, and BDC controlled BES with grid integrated at alternate PCI
- Fig. 5.3 Configuration of AC/DC microgrid consisting of DFIG-based WECS, double-stage SECS, and BDC controlled BES with grid integrated at alternate PCI
- Fig. 5.4 Identified operation modes of DFIG-SPV based AC/DC microgrids with grid integrated at alternate PCI
- Fig. 5.5 Selection criteria for computing status of S_{SSTS} in DFIG-SPV based AC/DC microgrids with grid integrated at alternate PCI
- Fig. 5.6 Selection criteria for computing status of G_{SSTS} in DFIG-SPV based AC/DC microgrids with grid integrated at alternate PCI
- Fig. 5.7 Operational strategy for DFIG-SPV based AC/DC microgrids with grid integrated at alternate PCI
- Fig. 5.8 Control scheme for RSC in DFIG-SPV based AC/DC microgrids with grid integrated at alternate PCI
- Fig. 5.9 Control scheme for SSC in DFIG-SPV based AC/DC microgrids with grid integrated at alternate PCI
- Fig. 5.10 Control scheme for GSC in DFIG-SPV based AC/DC microgrids with grid integrated at alternate PCI
- Fig. 5.11 Constant current injection based GSC control scheme for grid power smoothening
- Fig. 5.12 Exponential estimate based GSC control scheme for grid power smoothening
- Fig. 5.13 Ramp-rate limit based GSC control scheme for grid power smoothening
- Fig. 5.14 Screenshot for simulation of DFIG-SPV based AC/DC microgrids with grid integrated at alternate PCI in MATLAB
- Fig. 5.15 Snapshot of experimental prototype of DFIG-SPV based AC/DC microgrids with grid integrated at alternate PCI terminals
- Fig. 5.16 Simulation performance of AC/DC microgrid consisting of DFIG-based WECS, double-stage SECS, and BES with grid integrated at alternate PCI
- Fig. 5.17 MPPT performance of SPV array in AC/DC microgrid consisting of DFIG-based WECS, double-stage SECS, and BES with grid integrated at alternate PCI
- Fig. 5.18 Steady-state waveforms and indices of DFIG in AC/DC microgrid consisting of DFIG-based WECS, double-stage SECS, and BES with grid integrated at alternate PCI

- Fig. 5.19 Dynamic performance at varying wind speed and solar irradiation in AC/DC microgrid consisting of DFIG-based WECS, double-stage SECS, and BES with grid integrated at alternate PCI
- Fig. 5.20 Test results displaying uninterrupted operation and seamless transition in AC/DC microgrid consisting of DFIG-based WECS, double-stage SECS, and BES with grid integrated at alternate PCI at TP-I
- Fig. 5.21 Test results displaying uninterrupted operation and seamless transition in AC/DC microgrid consisting of DFIG-based WECS, double-stage SECS, and BES with grid integrated at alternate PCI at TP-II
- Fig. 5.22 Test results displaying uninterrupted operation and seamless transition in AC/DC microgrid consisting of DFIG-based WECS, double-stage SECS, and BES with grid integrated at alternate PCI at TP-III and TP-IV
- Fig. 5.23 Power quality performance at PCI-2 terminals in AC/DC microgrid consisting of DFIG-based WECS, double-stage SECS, and BES with grid integrated at alternate PCI
- Fig. 5.24 Power quality performance at PCI-1 terminals in AC/DC microgrid consisting of DFIG-based WECS, double-stage SECS, and BES with grid integrated at alternate PCI
- Fig. 5.25 Dynamic performance of AC/DC microgrid consisting of DFIG-based WECS, double-stage SECS, and BES with grid integrated at alternate PCI during load changes
- Fig. 5.26 Simulation performance of AC/DC microgrid consisting of DFIG-based WECS, single-stage SECS, and BDC controlled BES with grid integrated at alternate PCI during TP-I and TP-II
- Fig. 5.27 Simulation performance of AC/DC microgrid consisting of DFIG-based WECS, single-stage SECS, and BDC controlled BES with grid integrated at alternate PCI during TP-III and TP-IV
- Fig. 5.28 MPPT performance of SPV array in AC/DC microgrid consisting of DFIG-based WECS, single-stage SECS, and BDC controlled BES with grid integrated at alternate PCI
- Fig. 5.29 Steady-state waveforms and parameters of DFIG-based WECS in AC/DC microgrid consisting of DFIG-based WECS, single-stage SECS, and BDC controlled BES with grid integrated at alternate PCI
- Fig. 5.30 Dynamic performance at varying wind speed and solar irradiation in AC/DC microgrid consisting of DFIG-based WECS, single-stage SECS, and BDC controlled BES with grid integrated at alternate PCI
- Fig. 5.31 Test results displaying uninterrupted operation and seamless transition in AC/DC microgrid consisting of DFIG-based WECS, single-stage SECS, and BDC controlled BES with grid integrated at alternate PCI at TP-I
- Fig. 5.32 Test results displaying uninterrupted operation and seamless transition in AC/DC microgrid consisting of DFIG-based WECS, single-stage SECS, and BDC controlled BES with grid integrated at alternate PCI at TP-II

- Fig. 5.33 Test results displaying uninterrupted operation and seamless transition in AC/DC microgrid consisting of DFIG-based WECS, single-stage SECS, and BDC controlled BES with grid integrated at alternate PCI at TP-III and TP-IV
- Fig. 5.34 Power quality performance at PCI-2 terminals in AC/DC microgrid consisting of DFIG-based WECS, single-stage SECS, and BDC controlled BES with grid integrated at alternate PCI
- Fig. 5.35 Dynamic performance of AC/DC microgrid consisting of DFIG-based WECS, single-stage SECS, and BDC controlled BES with grid integrated at alternate PCI during load changes
- Fig. 5.36 Simulation performance of AC/DC microgrid consisting of DFIG-based WECS, double-stage SECS, and BDC controlled BES with grid integrated at alternate PCI
- Fig. 5.37 MPPT performance of SPV array in AC/DC microgrid consisting of DFIG-based WECS, double-stage SECS, and BDC controlled BES with grid integrated at alternate PCI
- Fig. 5.38 Steady-state waveforms and parameters of DFIG-based WECS in AC/DC microgrid consisting of DFIG-based WECS, double-stage SECS, and BDC controlled BES with grid integrated at alternate PCI
- Fig. 5.39 Dynamic performance at varying wind speed and solar irradiation in AC/DC microgrid consisting of DFIG-based WECS, double-stage SECS, and BDC controlled BES with grid integrated at alternate PCI
- Fig. 5.40 Test result displaying uninterrupted operation and seamless transition in AC/DC microgrid consisting of DFIG-based WECS, double-stage SECS, and BDC controlled BES with grid integrated at alternate PCI at TP-I
- Fig. 5.41 Test results displaying uninterrupted operation and seamless transition in AC/DC microgrid consisting of DFIG-based WECS, double-stage SECS, and BDC controlled BES with grid integrated at alternate PCI at TP-II
- Fig. 5.42 Test results displaying uninterrupted operation and seamless transition in AC/DC microgrid consisting of DFIG-based WECS, double-stage SECS, and BDC controlled BES with grid integrated at alternate PCI at TP-III and TP-IV
- Fig. 5.43 Power quality performance of AC/DC microgrid consisting of DFIG-based WECS, double-stage SECS, and BDC controlled BES with grid integrated at alternate PCI amidst abnormal AC load at PCI-2 terminals
- Fig. 5.44 Power quality performance of AC/DC microgrid consisting of DFIG-based WECS, double-stage SECS, and BDC controlled BES with grid integrated at alternate PCI amidst abnormal AC load at PCI-1 terminals
- Fig. 5.45 Dynamic performance of AC/DC microgrid consisting of DFIG-based WECS, double-stage SECS, and BDC controlled BES with grid integrated at alternate PCI during AC load changes at PCI-2
- Fig. 5.46 Dynamic performance of AC/DC microgrid consisting of DFIG-based WECS, double-stage SECS, and BDC controlled BES with grid integrated at alternate PCI during AC load changes at PCI-1 and DC load changes

- Fig. 5.47 Performance of constant current injection based GSC control for grid power smoothing amidst variation in wind speed, solar irradiation, and load power
- Fig. 5.48 Performance of exponential estimate based GSC control for grid power smoothing amidst variation in wind speed
- Fig. 5.49 Performance of exponential estimate based GSC control for grid power smoothing amidst variation in solar irradiation
- Fig. 5.50 Performance of exponential estimate based GSC control for grid power smoothing amidst variation in load power
- Fig. 5.51 Performance of ramp-rate limit based GSC control for grid power smoothing amidst variation in wind power
- Fig. 5.52 Performance of ramp-rate limit based GSC control for grid power smoothing amidst variation in SPV array power
- Fig. 5.53 Performance of ramp-rate limit based GSC control for grid power smoothing amidst variation in load power
- Fig. 6.1 Configuration of AC/DC microgrid consisting of DFIG-based WECS, double-stage SECS, DG-set and BES with grid integrated at alternate PCI and DG-set integrated at DFIG stator
- Fig. 6.2 Configuration of AC/DC microgrid consisting of DFIG-based WECS, single-stage SECS, DG-set and BDC controlled BES with grid integrated at alternate PCI and DG-set integrated at DFIG stator
- Fig. 6.3 Configuration of AC/DC microgrid consisting of DFIG-based WECS, double-stage SECS, DG-set and BDC controlled BES with grid integrated at alternate PCI and DG-set integrated at DFIG stator
- Fig. 6.4 Identified operation modes of DFIG-SPV-DG based AC/DC microgrids with grid integrated at alternate PCI and DG-set integrated at DFIG stator
- Fig. 6.5 Selection criteria for computing status of S_{SSTS} and G_{SSTS} in DFIG-SPV-DG based AC/DC microgrids with grid integrated at alternate PCI and DG-set integrated at DFIG stator
- Fig. 6.6 Selection criteria for computing status of D_{SSTS} in DFIG-SPV-DG based AC/DC microgrids with grid integrated at alternate PCI and DG-set integrated at DFIG stator
- Fig. 6.7 Operational strategy for DFIG-SPV-DG based AC/DC microgrids with grid integrated at alternate PCI and DG-set integrated at DFIG stator
- Fig. 6.8 Control scheme for GSC in DFIG-SPV-DG based AC/DC microgrid with grid integrated at alternate PCI and DG-set integrated at DFIG stator
- Fig. 6.9 Control scheme for RSC in DFIG-SPV-DG based AC/DC microgrids with grid integrated at alternate PCI and DG-set integrated at DFIG stator
- Fig. 6.10 Control scheme for SSC in DFIG-SPV-DG based AC/DC microgrids with grid integrated at alternate PCI and DG-set integrated at DFIG stator

- Fig. 6.11 Pictorial representation of power management scheme utilizing ToUEP mechanism in DFIG-SPV-DG based AC/DC microgrids with grid integrated at alternate PCI and DG-set integrated at DFIG stator
- Fig. 6.12 Screenshot for simulation of DFIG-SPV-DG based AC/DC microgrids with grid integrated at alternate PCI and DG-set integrated at DFIG stator in MATLAB
- Fig. 6.13 Snapshot of experimental prototype of DFIG-SPV-DG based AC/DC microgrids with grid integrated at alternate PCI and DG-set integrated at DFIG stator
- Fig. 6.14 Simulation performance of AC/DC microgrid consisting of DFIG-based WECS, double-stage SECS, DG-set and BES with grid integrated at alternate PCI and DG-set integrated at DFIG stator
- Fig. 6.15 MPPT performance of SPV array in AC/DC microgrid consisting of DFIG-based WECS, double-stage SECS, DG-set and BES with grid integrated at alternate PCI and DG-set integrated at DFIG stator
- Fig. 6.16 Dynamic performance at varying wind speed in AC/DC microgrid consisting of DFIG-based WECS, double-stage SECS, DG-set and BES with grid integrated at alternate PCI and DG-set integrated at DFIG stator
- Fig. 6.17 Dynamic performance at varying solar irradiation in AC/DC microgrid consisting of DFIG-based WECS, double-stage SECS, DG-set and BES with grid integrated at alternate PCI and DG-set integrated at DFIG stator
- Fig. 6.18 Test results displaying uninterrupted operation and seamless transition in AC/DC microgrid consisting of DFIG-based WECS, double-stage SECS, DG-set and BES with grid integrated at alternate PCI and DG-set integrated at DFIG stator during TP-I and TP-II
- Fig. 6.19 Test results displaying uninterrupted operation and seamless transition in AC/DC microgrid consisting of DFIG-based WECS, double-stage SECS, DG-set and BES with grid integrated at alternate PCI and DG-set integrated at DFIG stator during TP-III and TP-V
- Fig. 6.20 Test results displaying uninterrupted operation and seamless transition in AC/DC microgrid consisting of DFIG-based WECS, double-stage SECS, DG-set and BES with grid integrated at alternate PCI and DG-set integrated at DFIG stator during TP-IV
- Fig. 6.21 Test results displaying uninterrupted operation and seamless transition in AC/DC microgrid consisting of DFIG-based WECS, double-stage SECS, DG-set and BES with grid integrated at alternate PCI and DG-set integrated at DFIG stator during TP-VI
- Fig. 6.22 Test results displaying uninterrupted operation and seamless transition in AC/DC microgrid consisting of DFIG-based WECS, double-stage SECS, DG-set and BES with grid integrated at alternate PCI and DG-set integrated at DFIG stator during TP-VII and TP-VIII

- Fig. 6.23 Test results displaying uninterrupted operation and seamless transition in AC/DC microgrid consisting of DFIG-based WECS, double-stage SECS, DG-set and BES with grid integrated at alternate PCI and DG-set integrated at DFIG stator during TP-IX and TP-X
- Fig. 6.24 Power quality performance at PCI-1 terminals in AC/DC microgrid consisting of DFIG-based WECS, double-stage SECS, DG-set and BES with grid integrated at alternate PCI and DG-set integrated at DFIG stator
- Fig. 6.25 Power quality performance at PCI-2 terminals in AC/DC microgrid consisting of DFIG-based WECS, double-stage SECS, DG-set and BES with grid integrated at alternate PCI and DG-set integrated at DFIG stator
- Fig. 6.26 Dynamic performance of AC/DC microgrid consisting of DFIG-based WECS, double-stage SECS, DG-set and BES with grid integrated at alternate PCI and DG-set integrated at DFIG stator during load changes
- Fig. 6.27 Simulation performance of AC/DC microgrid consisting of DFIG-based WECS, single-stage SECS, DG-set and BDC controlled BES with grid integrated at alternate PCI and DG-set integrated at DFIG stator during mode transition scenarios
- Fig. 6.28 MPPT performance of SPV array in AC/DC microgrid consisting of DFIG-based WECS, single-stage SECS, DG-set and BDC controlled BES with grid integrated at alternate PCI and DG-set integrated at DFIG stator
- Fig. 6.29 Dynamic performance at varying wind speed in AC/DC microgrid consisting of DFIG-based WECS, single-stage SECS, DG-set and BDC controlled BES with grid integrated at alternate PCI and DG-set integrated at DFIG stator
- Fig. 6.30 Dynamic performance at varying solar irradiation in AC/DC microgrid consisting of DFIG-based WECS, single-stage SECS, DG-set and BDC controlled BES with grid integrated at alternate PCI and DG-set integrated at DFIG stator
- Fig. 6.31 Test results displaying uninterrupted operation and seamless transition in AC/DC microgrid consisting of DFIG-based WECS, single-stage SECS, DG-set and BDC controlled BES with grid integrated at alternate PCI and DG-set integrated at DFIG stator during TP-I and TP-II
- Fig. 6.32 Test results displaying uninterrupted operation and seamless transition in AC/DC microgrid consisting of DFIG-based WECS, single-stage SECS, DG-set and BDC controlled BES with grid integrated at alternate PCI and DG-set integrated at DFIG stator during TP-III and TP-V
- Fig. 6.33 Test results displaying uninterrupted operation and seamless transition in AC/DC microgrid consisting of DFIG-based WECS, single-stage SECS, DG-set and BDC controlled BES with grid integrated at alternate PCI and DG-set integrated at DFIG stator during TP-IV
- Fig. 6.34 Test results displaying uninterrupted operation and seamless transition in AC/DC microgrid consisting of DFIG-based WECS, single-stage SECS, DG-

- set and BDC controlled BES with grid integrated at alternate PCI and DG-set integrated at DFIG stator during TP-VI
- Fig. 6.35 Test results displaying uninterrupted operation and seamless transition in AC/DC microgrid consisting of DFIG-based WECS, single-stage SECS, DG-set and BDC controlled BES with grid integrated at alternate PCI and DG-set integrated at DFIG stator during TP-VII and TP-VIII
- Fig. 6.36 Test results displaying uninterrupted operation and seamless transition in AC/DC microgrid consisting of DFIG-based WECS, single-stage SECS, DG-set and BDC controlled BES with grid integrated at alternate PCI and DG-set integrated at DFIG stator during TP-IX and TP-X
- Fig. 6.37 Power quality performance at PCI-1 terminals in AC/DC microgrid consisting of DFIG-based WECS, single-stage SECS, DG-set and BDC controlled BES with grid integrated at alternate PCI and DG-set integrated at DFIG stator
- Fig. 6.38 Power quality performance at PCI-2 terminals in AC/DC microgrid consisting of DFIG-based WECS, single-stage SECS, DG-set and BDC controlled BES with grid integrated at alternate PCI and DG-set integrated at DFIG stator
- Fig. 6.39 Dynamic performance of AC/DC microgrid consisting of DFIG-based WECS, single-stage SECS, DG-set and BDC controlled BES with grid integrated at alternate PCI and DG-set integrated at DFIG stator during PCI-2 load changes
- Fig. 6.40 Dynamic performance of AC/DC microgrid consisting of DFIG-based WECS, single-stage SECS, DG-set and BDC controlled BES with grid integrated at alternate PCI and DG-set integrated at DFIG stator during PCI-1 load and LVDC load changes
- Fig. 6.41 Simulation performance of AC/DC microgrid consisting of DFIG-based WECS, double-stage SECS, DG-set and BDC controlled BES with grid integrated at alternate PCI and DG-set integrated at DFIG stator
- Fig. 6.42 MPPT performance of SPV array in AC/DC microgrid consisting of DFIG-based WECS, double-stage SECS, DG-set and BDC controlled BES with grid integrated at alternate PCI and DG-set integrated at DFIG stator
- Fig. 6.43 Dynamic performance at varying solar irradiation during DG-set connected state in AC/DC microgrid consisting of DFIG-based WECS, double-stage SECS, DG-set and BDC controlled BES with grid integrated at alternate PCI and DG-set integrated at DFIG stator
- Fig. 6.44 Dynamic performance at varying solar irradiation during grid connected state in AC/DC microgrid consisting of DFIG-based WECS, double-stage SECS, DG-set and BDC controlled BES with grid integrated at alternate PCI and DG-set integrated at DFIG stator
- Fig. 6.45 Test result displaying uninterrupted operation and seamless transition in AC/DC microgrid consisting of DFIG-based WECS, double-stage SECS, DG-set and BDC controlled BES with grid integrated at alternate PCI and DG-set integrated at DFIG stator during TP-I and TP-II

- Fig. 6.46 Test result displaying uninterrupted operation and seamless transition in AC/DC microgrid consisting of DFIG-based WECS, double-stage SECS, DG-set and BDC controlled BES with grid integrated at alternate PCI and DG-set integrated at DFIG stator during TP-III and TP-V
- Fig. 6.47 Test result displaying uninterrupted operation and seamless transition in AC/DC microgrid consisting of DFIG-based WECS, double-stage SECS, DG-set and BDC controlled BES with grid integrated at alternate PCI and DG-set integrated at DFIG stator during TP-IV
- Fig. 6.48 Test result displaying uninterrupted operation and seamless transition in AC/DC microgrid consisting of DFIG-based WECS, double-stage SECS, DG-set and BDC controlled BES with grid integrated at alternate PCI and DG-set integrated at DFIG stator during TP-VI
- Fig. 6.49 Test result displaying uninterrupted operation and seamless transition in AC/DC microgrid consisting of DFIG-based WECS, double-stage SECS, DG-set and BDC controlled BES with grid integrated at alternate PCI and DG-set integrated at DFIG stator during TP-VII and TP-VIII
- Fig. 6.50 Test result displaying uninterrupted operation and seamless transition in AC/DC microgrid consisting of DFIG-based WECS, double-stage SECS, DG-set and BDC controlled BES with grid integrated at alternate PCI and DG-set integrated at DFIG stator during TP-IX and TP-X
- Fig. 6.51 Power quality performance at PCI-2 terminals in AC/DC microgrid consisting of DFIG-based WECS, double-stage SECS, DG-set and BDC controlled BES with grid integrated at alternate PCI and DG-set integrated at DFIG stator
- Fig. 6.52 Power quality performance at PCI-1 terminals in AC/DC microgrid consisting of DFIG-based WECS, double-stage SECS, DG-set and BDC controlled BES with grid integrated at alternate PCI and DG-set integrated at DFIG stator
- Fig. 6.53 Dynamic performance of AC/DC microgrid consisting of DFIG-based WECS, double-stage SECS, DG-set and BDC controlled BES with grid integrated at alternate PCI and DG-set integrated at DFIG stator during load changes
- Fig. 6.54 Performance of incentivized control in grid-integrated state through ToUEP mechanism
- Fig. 7.1 Configuration of multiple-source DFIG-SPV based standalone AC/DC microgrid with additional BSC
- Fig. 7.2 Configuration of multiple-source DFIG-SPV based standalone AC/DC microgrid without additional BSC
- Fig. 7.3 Control scheme for BSC in multiple-source DFIG-SPV based standalone AC/DC microgrid with additional BSC
- Fig. 7.4 Control scheme for ILC in multiple-source DFIG-SPV based standalone AC/DC microgrid with additional BSC
- Fig. 7.5 Control scheme for RSC of q^{th} -DFIG in multiple-source DFIG-SPV based standalone AC/DC microgrid with additional BSC

- Fig. 7.6 Control scheme for SSC of q^{th} -DFIG in multiple-source DFIG-SPV based standalone AC/DC microgrid with additional BSC
- Fig. 7.7 Control scheme for ILC in multiple-source DFIG-SPV based standalone AC/DC microgrid without additional BSC
- Fig. 7.8 Screenshot for simulation of multiple-source DFIG-SPV based standalone AC/DC microgrid with additional BSC in MATLAB
- Fig. 7.9 Screenshot for simulation of multiple-source DFIG-SPV based standalone AC/DC microgrid without additional BSC in MATLAB
- Fig. 7.10 Snapshot of experimental prototype of multiple-source DFIG-SPV based standalone AC/DC microgrids
- Fig. 7.11 Simulation performance of multiple-source DFIG-SPV based standalone AC/DC microgrid with additional BSC during mode transition scenarios
- Fig. 7.12 Simulation performance of multiple-source DFIG-SPV based standalone AC/DC microgrid with additional BSC amidst variations in microgrid entities connected to DC subgrid
- Fig. 7.13 Dynamic performance at varying wind speed in multiple-source DFIG-SPV based standalone AC/DC microgrid with additional BSC
- Fig. 7.14 Dynamic performance at varying solar irradiation in multiple-source DFIG-SPV based standalone AC/DC microgrid with additional BSC
- Fig. 7.15 Test results displaying uninterrupted operation and seamless transition in multiple-source DFIG-SPV based standalone AC/DC microgrid with additional BSC
- Fig. 7.16 Dynamic performance amidst AC load variations in multiple-source DFIG-SPV based standalone AC/DC microgrid with additional BSC
- Fig. 7.17 Power quality performance in multiple-source DFIG-SPV based standalone AC/DC microgrid with additional BSC
- Fig. 7.18 Dynamic performance amidst DC load variations in multiple-source DFIG-SPV based standalone AC/DC microgrid with additional BSC
- Fig. 7.19 Simulation performance of multiple-source DFIG-SPV based standalone AC/DC microgrid without additional BSC during mode transition scenarios
- Fig. 7.20 Simulation performance of multiple-source DFIG-SPV based standalone AC/DC microgrid without additional BSC amidst variations in wind speed
- Fig. 7.21 Simulation performance of multiple-source DFIG-SPV based standalone AC/DC microgrid without additional BSC amidst abnormal AC load
- Fig. 7.22 Dynamic performance at varying wind speed in multiple-source DFIG-SPV based standalone AC/DC microgrid without additional BSC
- Fig. 7.23 Dynamic performance at varying solar irradiation in multiple-source DFIG-SPV based standalone AC/DC microgrid without additional BSC
- Fig. 7.24 Test results displaying uninterrupted operation and seamless transition in multiple-source DFIG-SPV based standalone AC/DC microgrid without additional BSC

- Fig. 7.25 Dynamic performance amidst AC load variations in multiple-source DFIG-SPV based standalone AC/DC microgrid without additional BSC
- Fig. 7.26 Power quality performance in multiple-source DFIG-SPV based standalone AC/DC microgrid without additional BSC
- Fig. 7.27 Dynamic performance amidst DC load variations in multiple-source DFIG-SPV based standalone AC/DC microgrid without additional BSC
- Fig. 8.1 Configuration of multiple-source DFIG-SPV based AC/DC microgrid with grid integrated at DFIGs' stator terminals
- Fig. 8.2 Configuration of multiple-source DFIG-SPV based AC/DC microgrid with grid integrated at alternate interconnection terminals
- Fig. 8.3 Configuration of multiple-source DFIG-SPV based AC/DC microgrid with grid integrated at alternate interconnection terminals and DG-set integrated at DFIGs' stator terminals
- Fig. 8.4 Control scheme for ILC in multiple-source DFIG-SPV based AC/DC microgrid with grid integrated at DFIGs' stator terminals
- Fig. 8.5 Control scheme for ILC in multiple-source DFIG-SPV based AC/DC microgrid with grid integrated at alternate interconnection terminals
- Fig. 8.6 Control scheme for GSC in multiple-source DFIG-SPV based AC/DC microgrid with grid integrated at alternate interconnection terminals
- Fig. 8.7 Control scheme for ILC in multiple-source DFIG-SPV-DG based AC/DC microgrid with grid integrated at alternate interconnection terminals and DG-set integrated at DFIGs' stator terminals
- Fig. 8.8 Screenshot for simulation of multiple-source DFIG-SPV based AC/DC microgrid with grid integrated at DFIGs' stator terminals in MATLAB
- Fig. 8.9 Screenshot for simulation of multiple-source DFIG-SPV based AC/DC microgrid with grid integrated at alternate interconnection terminals in MATLAB
- Fig. 8.10 Screenshot for simulation of multiple-source DFIG-SPV based AC/DC microgrid with grid integrated at alternate interconnection terminals and DG-set integrated at DFIGs' stator terminals in MATLAB
- Fig. 8.11 Snapshot of experimental setup of multiple-source DFIG-SPV based grid-integrated AC/DC microgrids
- Fig. 8.12 Simulation performance of multiple-source DFIG-SPV based AC/DC microgrid with grid integrated at DFIGs' stator terminals during mode transition scenarios
- Fig. 8.13 Simulation performance of multiple-source DFIG-SPV based AC/DC microgrid with grid integrated at DFIGs' stator terminals amidst variations in microgrid entities connected to AC subgrid and DC subgrid
- Fig. 8.14 Simulation performance of multiple-source DFIG-SPV based AC/DC microgrid with grid integrated at DFIGs' stator terminals amidst variations in AC load

- Fig. 8.15 Simulation performance of multiple-source DFIG-SPV based AC/DC microgrid with grid integrated at DFIGs' stator terminals displaying harmonics spectra of various signals at abnormal AC load scenario
- Fig. 8.16 Dynamic performance at varying wind speed in multiple-source DFIG-SPV based AC/DC microgrid with grid integrated at DFIGs' stator terminals
- Fig. 8.17 Dynamic performance at varying solar irradiation in multiple-source DFIG-SPV based AC/DC microgrid with grid integrated at DFIGs' stator terminals
- Fig. 8.18 Test results displaying uninterrupted operation and seamless transition at the DFIG-side in multiple-source DFIG-SPV based AC/DC microgrid with grid integrated at DFIGs' stator terminals
- Fig. 8.19 Test results displaying uninterrupted operation and seamless transition at the grid-side in multiple-source DFIG-SPV based AC/DC microgrid with grid integrated at DFIGs' stator terminals
- Fig. 8.20 Dynamic performance amidst AC load variations in multiple-source DFIG-SPV based AC/DC microgrid with grid integrated at DFIGs' stator terminals
- Fig. 8.21 Power quality performance in multiple-source DFIG-SPV based AC/DC microgrid with grid integrated at DFIGs' stator terminals
- Fig. 8.22 Dynamic performance amidst DC load variations in multiple-source DFIG-SPV based AC/DC microgrid with grid integrated at DFIGs' stator terminals
- Fig. 8.23 Simulation performance of multiple-source DFIG-SPV based AC/DC microgrid with grid integrated at alternate interconnection terminals during mode transition scenarios
- Fig. 8.24 Simulation performance of multiple-source DFIG-SPV based AC/DC microgrid with grid integrated at alternate interconnection terminals at variations in microgrid entities connected to AC subgrid and DC subgrid
- Fig. 8.25 Simulation performance of multiple-source DFIG-SPV based AC/DC microgrid with grid integrated at alternate interconnection terminals amidst variations in AC load
- Fig. 8.26 Simulation performance of multiple-source DFIG-SPV based AC/DC microgrid with grid integrated at alternate interconnection terminals displaying harmonics spectra of various signals at abnormal AC load scenario
- Fig. 8.27 Dynamic performance at varying wind speed in multiple-source DFIG-SPV based AC/DC microgrid with grid integrated at alternate interconnection terminals
- Fig. 8.28 Dynamic performance at varying solar irradiation in multiple-source DFIG-SPV based AC/DC microgrid with grid integrated at alternate interconnection terminals
- Fig. 8.29 Test results displaying uninterrupted operation and seamless transition at the DFIG-side in multiple-source DFIG-SPV based AC/DC microgrid with grid integrated at alternate interconnection terminals

- Fig. 8.30 Test results displaying uninterrupted operation and seamless transition at the grid-side in multiple-source DFIG-SPV based AC/DC microgrid with grid integrated at alternate interconnection terminals
- Fig. 8.31 Dynamic performance amidst AC load variations in multiple-source DFIG-SPV based AC/DC microgrid with grid integrated at alternate interconnection terminals
- Fig. 8.32 Power quality performance in multiple-source DFIG-SPV based AC/DC microgrid with grid integrated at alternate interconnection terminals
- Fig. 8.33 Dynamic performance amidst DC load variations in multiple-source DFIG-SPV-DG based AC/DC microgrid with grid integrated at alternate interconnection terminals
- Fig. 8.34 Simulation performance of multiple-source DFIG-SPV-DG based AC/DC microgrid with grid integrated at alternate interconnection terminals and DG-set integrated at DFIGs' stator terminals during DFIG and DG-set related mode transition scenarios
- Fig. 8.35 Simulation performance of multiple-source DFIG-SPV-DG based AC/DC microgrid with grid integrated at alternate interconnection terminals and DG-set integrated at DFIGs' stator terminals during grid related mode transition scenarios
- Fig. 8.36 Simulation performance of multiple-source DFIG-SPV-DG based AC/DC microgrid with grid integrated at alternate interconnection terminals and DG-set integrated at DFIGs' stator terminals displaying optimal consumption of diesel fuel at varying wind and load powers conditions
- Fig. 8.37 Simulation performance of multiple-source DFIG-SPV-DG based AC/DC microgrid with grid integrated at alternate interconnection terminals and DG-set integrated at DFIGs' stator terminals displaying constant power injection at utility grid irrespective of system power changes
- Fig. 8.38 Simulation performance of multiple-source DFIG-SPV-DG based AC/DC microgrid with grid integrated at alternate interconnection terminals and DG-set integrated at DFIGs' stator terminals displaying harmonics spectra of various signals at abnormal AC load scenario
- Fig. 8.39 Dynamic performance at varying wind speed in multiple-source DFIG-SPV-DG based AC/DC microgrid with grid integrated at alternate interconnection terminals and DG-set integrated at DFIGs' stator terminals
- Fig. 8.40 Dynamic performance at varying solar irradiation in multiple-source DFIG-SPV-DG based AC/DC microgrid with grid integrated at alternate interconnection terminals and DG-set integrated at DFIGs' stator terminals
- Fig. 8.41 Test results displaying uninterrupted operation and seamless transition at the DFIG-side in multiple-source DFIG-SPV-DG based AC/DC microgrid with grid integrated at alternate interconnection terminals and DG-set integrated at DFIGs' stator terminals

- Fig. 8.42 Test results displaying uninterrupted operation and seamless transition at the grid-side in multiple-source DFIG-SPV-DG based AC/DC microgrid with grid integrated at alternate interconnection terminals and DG-set integrated at DFIGs' stator terminals
- Fig. 8.43 Test results displaying uninterrupted operation and seamless transition at the DG-side in multiple-source DFIG-SPV-DG based AC/DC microgrid with grid integrated at alternate interconnection terminals and DG-set integrated at DFIGs' stator terminals
- Fig. 8.44 Dynamic performance amidst AC load variations in multiple-source DFIG-SPV-DG based AC/DC microgrid with grid integrated at alternate interconnection terminals and DG-set integrated at DFIGs' stator terminals
- Fig. 8.45 Power quality performance in multiple-source DFIG-SPV-DG based AC/DC microgrid with grid integrated at alternate interconnection terminals and DG-set integrated at DFIGs' stator terminals
- Fig. 8.46 Dynamic performance amidst DC load variations in multiple-source DFIG-SPV-DG based AC/DC microgrid with grid integrated at alternate interconnection terminals and DG-set integrated at DFIGs' stator terminals
- Fig. B.1 Circuitry for optical isolation and amplification of PWM signals
- Fig. B.2 Snapshot of PCB for realizing optical isolation and amplification of PWM signals
- Fig. B.3 Circuitry for voltage signal sensing and conditioning
- Fig. B.4 Snapshot of PCB for realizing voltage signal sensing and conditioning
- Fig. B.5 Circuitry for current signal sensing and conditioning
- Fig. B.6 Snapshot of PCB for realizing current signal sensing and conditioning

LIST OF TABLES

Table 3.1	Possible transition phases for DFIG-SPV based standalone AC/DC microgrids
Table 4.1	Possible transition phases for DFIG-SPV based AC/DC microgrids with grid integrated at DFIG stator
Table 4.2	System parameters for DFIG-SPV based AC/DC microgrids with grid integrated at DFIG stator
Table 4.3	Summary of control targets for enhanced operation at non-ideal grid
Table 5.1	Possible transition phases for DFIG-SPV based AC/DC microgrids with grid integrated at alternate PCI
Table 5.2	System parameters for DFIG-SPV based AC/DC microgrids with grid integrated at alternate PCI
Table 6.1	Possible transition phases for DFIG-SPV-DG based AC/DC microgrids with grid integrated at alternate PCI and DG-set integrated at DFIG stator
Table 6.2	System parameters for DFIG-SPV-DG based AC/DC microgrids with grid integrated at alternate PCI and DG-set integrated at DFIG stator
Table 7.1	System parameters for multiple-source DFIG-SPV based standalone AC/DC microgrids
Table 8.1	System parameters for multiple-source DFIG-SPV based grid-integrated AC/DC microgrids

LIST OF ABBREVIATIONS

AC	Alternating Current
APSA	Affine Projection Sign Algorithm
Arc-NLMS	Arctangent Normalized Least Mean Square
ATLMLS	Arctangent Least Mean Logarithmic Square
AVR	Automatic Voltage Regulator
BDC	DC–DC Bidirectional Converter
BES	Battery Energy Storage
BEVC	DC–DC Bidirectional Converter for Electric Vehicle Charging
BKC	DC–DC Buck Converter
BSC	Battery-side Converter
BTC	DC–DC Boost Converter
<i>Cext</i> SOGI-HSS	Cross-feedback Extended Second Order Generalized Integrator based Harmonics Sequence Separator
DBR	Diode Bridge Rectifier
DC	Direct Current
DFIG	Doubly-fed Induction Generator
DG	Diesel Generator
DSO	Digital Signal Oscilloscope
D _{SSTS}	DG-side Solid State Transition Switch
DT	DFIG-side Control Target for Multi-target Control at Non-ideal Grid
ES	Energy Storage
EV	Electric Vehicle
<i>ext</i> SOGI	Extended Second Order Generalized Integrator
GMBZ-AF	Generic Modified Blake-Zisserman Adaptive Filter
GSC	Grid-side Converter
G _{SSTS}	Grid-side Solid State Transition Switch
GT	Grid-side Control Target for Multi-target Control at Non-ideal Grid
HGI	Higher-order Generalized Integrator
HPRE	High Power Ramp Event
IEEE	Institute of Electrical and Electronics Engineers
IGBT	Insulated Gate Bipolar Transistor
ILC	Interlinking Converter
InC	Incremental Conductance
LVDC	Low Voltage Direct Current
LVUF	Line Voltage Unbalance Factor
MPP	Maximum Power Point

MPPT	Maximum Power Point Tracking
MRAS	Model Reference Adaptive Scheme
MRHGI-HE	Multi-resonant Higher-order Generalized Integrator based Harmonic Estimator
MVDC	Medium Voltage Direct Current
NLMAT	Normalized Least Mean Absolute Third
NMCC	Normalized Maximum Correntropy Criterion
OFU	Optimal Fuel Utilization
OTSR	Optimal Tip Speed Ratio
OTT	Optimal Turbine Torque
PCI	Point of Common Interconnection
PI	Proportional Integral
PLL	Phase Locked Loop
PMS	Power Management Scheme
PMSG	Permanent Magnet Synchronous Generator
P&O	Perturb and Observe
PQ	Power Quality
PQA	Power Quality Analyzer
PR	Proportional Resonant
PRR	Power Ramp Rate
PSF	Power Signal Feedback
PWM	Pulse Width Modulation
RES	Renewable Energy Source
RLMAT	Robust Least Mean Absolute Third
RMS	Root Mean Square
RRL	Ramp Rate Limit
RSC	Rotor-side Converter
SCIG	Squirrel Cage Induction Generator
SCIM	Squirrel Cage Induction Motor
SCR	Silicon Controlled Rectifier
SECS	Solar Energy Conversion System
SG	Synchronous Generator
SSC	Stator-side Converter
SPV	Solar Photovoltaic
SsSTS	Stator-side Solid State Transition Switch
THD	Total Harmonic Distortion
ToUEP	Time of Use Electricity Price
TP	Transition Phase
UPF	Unity Power Factor

VSC	Voltage Source Converter
VZA-LMS	Versoria Zero-Attraction Least Mean Square
WECS	Wind Energy Conversion System
WRIG	Wound Rotor Induction Generator
WRSG	Wound Rotor Synchronous Generator
WT	Wind Turbine

LIST OF SYMBOLS

β	Pitch angle of wind turbine blade (rad.)
χ	Air density
B_r	Blade radius of wind turbine (m)
C_{bkc}	BKC capacitor (F)
C_{dc}	DC-link capacitor (F)
C_f	Ripple filter capacitor (F)
C_p	Coefficient of power from wind turbine
C_{pmax}	Maximum coefficient of power from wind turbine
C_{pv}	Capacitor connected across SPV array (F)
C_t	Coefficient of torque from wind turbine
δ	Percentage of Voltage Ripple across Two DC Link Capacitors (V)
D_{bkc}	Diode of BKC
D_{btc}	Diode of BTC
D_{pv}	Protection diode of SPV array
D_{sgnl}	DG-side signal to determine necessity for connection of DG-set
D_0, D_1	Disconnected and connected state of D_{SSTS}
Δi_{rpBDC}	Ripple content in inductor current of BDC (A)
Δi_{rpBKC}	Ripple content in inductor current of BKC (A)
Δi_{rpBTC}	Ripple content in inductor current of BTC (A)
Δi_{rpSSC}	Ripple content in inductor current of SSC (A)
ΔI_{pv}	Change in SPV array current after one sample instant (A)
ΔV_{pv}	Change in SPV array voltage after one sample instant (V)
ΔV	Fixed step increment/decrement in SPV array voltage for MPPT algorithm (V)
e	Error signal for adaptive filtering techniques
ε_{dc}	Error between reference and sensed DC-link voltages (V)
ε_{ω}	Error between reference and sensed DFIG rotor speeds (rad./s)
ε_{ψ}	Error between stator fluxes for MRAS algorithm (Wb)
ε_{vdc}	Error between reference and sensed LVDC voltages (V)
ε_{vs}	Error between reference and sensed DFIG stator voltages (V)
f	Rated frequency of system (Hz)
f_d	Frequency of DG-set voltage (Hz)
f_g	Frequency of grid voltage (Hz)
f_i	Frequency of PCI-1 voltage (Hz)
f_L	Frequency of PCI-2 voltage (Hz)
f_s	Frequency of DFIG stator voltage (Hz)

f_{ih}	Frequency error tolerance in voltage as per IEEE 1547 (Hz)
f_{swBDC}	Switching frequency of BDC (Hz)
f_{swBKC}	Switching frequency of BKC (Hz)
f_{swBTC}	Switching frequency of BTC (Hz)
f_{swSSC}	Switching frequency of SSC (Hz)
G_r	Gearbox ratio of wind turbine
G_{sgnl}	Grid-side signal to determine availability of utility grid
G_0, G_1	Disconnected and connected state of G_{SSTS}
G_{pv}	Solar irradiation incident at SPV array (W/m^2)
h_{dc}	Overload factor for DC-link capacitance
h_{SSC}	Overload factor for L_{iS} design
L_{iB}	Interfacing inductance for BSC (H)
L_{iG}	Interfacing inductance for GSC (H)
L_{iI}	Interfacing inductance for ILC (H)
L_{iS}	Interfacing inductance for SSC (H)
L_{bdc}	Inductance for BDC (H)
L_{bevc}	Inductance for BEVC (H)
L_{bkc}	Inductance for BKC (H)
L_{btc}	Inductance for BTC (H)
Q_g	Grid reactive power (VAR)
Q_l	PCI-1 side AC load reactive power (VAR)
Q_L	PCI-2 side AC load reactive power (VAR)
Q_r	DFIG rotor reactive power (VAR)
Q_s	DFIG stator reactive power (VAR)
I_b	BES current (A)
i_{bsc}	BSC current (A)
i_c	PCI-1 side shunt current (A)
i_C	PCI-2 side shunt current (A)
i_d	DG-set current (A)
I_{ev}	EV load current (A)
i_g	Grid current (A)
i_{ilc}	Interlinking converter current (A)
i_l	PCI-1 side AC load current (A)
i_L	PCI-2 side AC load current (A)
I_{mp_array}	MPP current of SPV array at standard test conditions (A)
I_{mp_panel}	MPP current of SPV panel at standard test conditions (A)
I_{ohv}	LVDC load current (A)

I_{omv}	MVDC load current (A)
I_{pv}	SPV array current (A)
i_r	DFIG rotor current (A)
i_s	DFIG stator current (A)
I_{sc_array}	Short circuit current rating of SPV array at standard test conditions (A)
I_{sc_panel}	Short circuit current rating of SPV panel at standard test conditions (A)
I_{swRSC}	Current rating of IGBT switches in RSC (A)
I_{swSSC}	Current rating of IGBT switches in SSC (A)
i_w	Current injected by each WECS in multiple-source AC/DC microgrid
k	Represents signal at the present sample instant
k_{dc}	Measure of energy variation in DC-link capacitor during dynamics
k_i	Integral gain for PI regulator
k_p	Proportional gain for PI/PR regulator
k_r	Resonant gain for PR regulator
kVA_{RSC}	kVA rating of RSC
kVA_{SSC}	kVA rating of SSC
L_{bdc}	BDC inductor (H)
L_{bkc}	BKC inductor (H)
L_{btc}	BTC inductor (H)
L_{iG}	GSC interfacing inductor (H)
L_{iS}	SSC interfacing inductor (H)
L_m	DFIG magnetizing inductance (H)
L_r	DFIG rotor inductance (H)
L_s	DFIG stator inductance (H)
$L_{\sigma r}$	DFIG rotor leakage inductance (H)
$L_{\sigma s}$	DFIG stator leakage inductance (H)
λ	Tip speed ratio of wind turbine
λ_i	Intermediate tip speed signal in wind turbine modelling
λ_o	Optimal tip speed ratio of wind turbine
m	Amplitude modulation index of VSC
$\mu, \sigma, \gamma, \rho$	Constants used in adaptive filtering techniques
$n_{parallel}$	Number of parallel connected SPV strings in an SPV array
$N_{rt/st}$	DFIG rotor to stator turns ratio
n_{series}	Number of series connected SPV panels in an SPV string
Ω_t	Rotational speed of wind turbine (rad./s)
Ω_m	Rotational speed of DFIG mech. (rad./s)
Ω_{mmax}	Maximum rotational speed of DFIG mech. (rad./s)

Ω_s	Synchronous speed of DFIG mech. (rad./s)
ω_e	Reference angular speed corresponding to rated frequency (rad./s)
ω_m	Rotational speed of DFIG elec. (rad./s)
ω_{PR}	Bandwidth for PR regulator (rad./s)
p	DFIG pole pairs
P_b	BES power (W)
P_g	Grid active power (W)
P_l	PCI-1 side AC load active power (W)
P_L	PCI-2 side AC load active power (W)
P_m	Power from wind turbine (W)
P_{mmax}	Rated power from wind turbine (W)
P_{pv}	SPV array power (W)
P_r	DFIG rotor active power (W)
P_s	DFIG stator active power (W)
P_{SSC}	SSC active power (W)
P_w	Power injected by each WECS in multiple-source AC/DC microgrid
R_f	Ripple filter resistor (Ω)
R_r	DFIG rotor resistance (Ω)
R_s	DFIG stator resistance (Ω)
s	Laplace operator
S_0, S_l	Disconnected and connected state of S _{SSTS}
S_{bkc}	IGBT switch of BKC
S_{btc}	IGBT switch of BTC
S_{bk}, S_{bt}	IGBT switches of BDC
ψ_s	Stator flux (Wb)
s_l	DFIG operating slip
S_{sgnl}	DFIG stator-side signal to determine generation possibility from WECS
$S_{w1} - S_{w6}$	IGBT switches of RSC
$S_{w7} - S_{w12}$	IGBT switches of SSC
$S_{w13} - S_{w18}$	IGBT switches of GSC
t_{dc}	Recovery time for DC-link capacitor to regain steady-state (s)
T_m	Torque from wind turbine (Nm)
T_{PR}	Transfer function for PR regulator
T_{pv}	Temperature incident at SPV array ($^{\circ}$ C)
θ_d	Phase angle of DG-set voltage (rad.)
θ_e	Reference phase angle corresponding to rated frequency (rad.)
θ_{ed}	Error in phase angles of PCI-2 voltages and DG-set voltages (rad.)

θ_{eg}	Error in phase angles of PCI-1/2 voltages and grid voltages (rad.)
θ_{es}	Error in phase angles of PCI-1 voltages and DFIG stator voltages (rad.)
θ_g	Phase angle of grid voltage (rad.)
θ_l	Phase angle of PCI-1 voltage (rad.)
θ_m	DFIG rotor position electrical (rad.)
θ_{m_mech}	DFIG rotor position mechanical (rad.)
θ_r	DFIG slip angle (rad.)
θ_s	Phase angle of DFIG stator flux (rad.)
θ_{st}	Phase angle of DFIG stator voltage (rad.)
θ_{th}	Phase angle error tolerance in voltage as per IEEE 1547 (rad.)
u	Unit sinusoid
V_b	BES voltage (V)
v_d	DG-set voltage (V)
V_{dc}	DC-link voltage (V)
V_{dcB}	DC-link voltage across BSC (V)
V_{dcq}	DC-link voltage across q^{th} -DFIG in multiple-source AC/DC microgrid (V)
V_{dpk}	Amplitude of DG-set voltage (V)
V_{ed}	Error in amplitudes of PCI-2 voltages and DG-set voltages (V)
V_{eg}	Error in amplitudes of PCI-1/2 voltages and grid voltages (V)
V_{es}	Error in amplitudes of PCI-1 voltages and DFIG stator voltages (V)
v_g	Grid voltage (V)
V_{gpk}	Amplitude of grid voltage (V)
v_l	PCI-1 voltage (V)
v_L	PCI-2 voltage (V)
V_{lpk}	Amplitude of PCI-1 voltage (V)
V_{Lpk}	Amplitude of PCI-2 voltage (V)
V_{mp_array}	MPP voltage of SPV array at standard test conditions (V)
V_{mp_panel}	MPP voltage of SPV panel at standard test conditions (V)
V_{oc_array}	Open circuit voltage rating of SPV array at standard test conditions (V)
V_{oc_panel}	Open circuit voltage rating of SPV panel at standard test conditions (V)
V_{olv}	LVDC bus voltage (V)
V_{pk}	Amplitude of AC voltage (V)
V_{pv}	SPV array voltage (V)
V_{ref}	SPV array reference voltage for MPPT (V)
v_s	DFIG stator voltage (V)
V_{spk}	Amplitude of DFIG stator voltage (V)
V_{swRSC}	Voltage rating of IGBT switches in RSC (V)

V_{swSSC}	Voltage rating of IGBT switches in SSC (V)
V_{th}	Amplitude error tolerance in voltage as per IEEE 1547 (V)
v_w	Sensed voltages across WECSs in multiple-source AC/DC microgrids (V)
V_w	Wind speed (m/s)
V_{wmax}	Rated wind speed (m/s)
VF_{dc}	Variation factor in DC-link capacitor
ξ	Weight component (A)
X_m	DFIG magnetizing reactance (Ω)

Subscripts

abc	Three phase entities
$\alpha\beta$	Stationary reference frame coordinates
dq	Synchronous reference frame coordinates
DQ	Rotor reference frame coordinates
$1, 2, 3 \dots q$	Different units of DFIGs in multiple-source AC/DC microgrids
$1, 2, 3 \dots t$	Different units of SPV arrays in multiple-source AC/DC microgrids
$1+, 5-$	Positive sequence fundamental frequency component, negative sequence fifth harmonic frequency component, etc.

Superscripts

*	Reference entities
$1+, 5-$	Signal referred to reference frame rotating with $+\omega_{syn}$ speed, $-5 \omega_{syn}$ speed, etc.